SANDIA REPORT
SAND2015-2484
Unclassified Unlimited Release
Printed April 2015

Advance Liquid Metal Reactor Discrete Dynamic Event Tree/Bayesian Network Analysis and Incident Management Guidelines (Risk Management for Sodium Fast Reactors)

Matthew R. Denman, Katrina M. Groth, Jeff Cardoni, Tim Wheeler

Prepared by
Sandia National Laboratories
Albuquerque, New Mexico 87185 and Livermore, California 94550

Sandia National Laboratories is a multi-program laboratory managed and operated by Sandia Corporation, a wholly owned subsidiary of Lockheed Martin Corporation, for the U.S. Department of Energy's National Nuclear Security Administration under contract DE-AC04-94AL85000.

Issued by Sandia National Laboratories, operated for the United States Department of Energy by Sandia Corporation.

Available to DOE and DOE contractors from
U.S. Department of Energy
Office of Scientific and Technical Information
P.O. Box 62
Oak Ridge, TN 37831

Telephone: (865) 576-8401
Facsimile: (865) 576-5728
E-Mail: reports@adonis.osti.gov
Online ordering: http://www.osti.gov/bridge

Available to the public from
U.S. Department of Commerce
National Technical Information Service
5285 Port Royal Rd.
Springfield, VA 22161

Telephone: (800) 553-6847
Facsimile: (703) 605-6900
E-Mail: orders@ntis.fedworld.gov
Online order: http://www.ntis.gov/help/ordermethods.asp?loc=7-4-0#online

SAND2015-2484
Unclassified-Unlimited Release
Printed April 2015

Advance Liquid Metal Reactor Discrete Dynamic Event Tree/Bayesian Network Analysis and Incident Management Guidelines (Risk Management for Sodium Fast Reactors) (Risk Management for Sodium Fast Reactors)

Matthew R Denman, Katrina M. Groth, Jeff Cardoni, Tim Wheeler
Sandia National Laboratories
P.O. Box 5800
Albuquerque, New Mexico 87185-MS0748

Abstract

Accident management is an important component to maintaining risk at acceptable levels for all complex systems, such as nuclear power plants. With the introduction of self-correcting, or inherently safe, reactor designs the focus has shifted from management by operators to allowing the system's design to manage the accident. Inherently and passively safe designs are laudable, but nonetheless extreme boundary conditions can interfere with the design attributes which facilitate inherent safety, thus resulting in unanticipated and undesirable end states. This report examines an inherently safe and small sodium fast reactor experiencing a beyond design basis seismic event with the intend of exploring two issues: (1) can human intervention either improve or worsen the potential end states and (2) can a Bayesian Network be constructed to infer the state of the reactor to inform (1).

ACKNOWLEDGEMENTS

The authors would like to acknowledge the U.S. Department of Energy's Office of Nuclear Energy for funding this research through Work Package SR-14SN100303 under the Advanced Reactor Concepts program. The authors also acknowledge the PRA teams at Argonne National Laboratory, Oak Ridge National Laboratory, and Idaho National Laboratory for their continued contributions to the advanced reactor PRA mission area.

CONTENTS

FIGURES

TABLES

ACRONYMS

ADHX	Air dump heat exchanger
ANL	Argonne National Laboratory
BN	Bayesian Network
BOP	Balance of Plant
CR	Control Rod
CS	Core Sloshing
DET	Dynamic Event Tree
DDET	Discrete Dynamic Event Tree
DHRS	Decay Heat Removal System
DRACS	Direct Reactor Auxiliary Cooling System
DOE	Department of Energy
DSS	Decision support system
EOP	Emergency Operating Procedures
EM	Electromagnetic (Pump)
EMP	Electromagnetic Pump
I&C	Instrumentation and Control
LOF	Loss of Flow
MC	Monte Carlo (sampling)
NRC	Nuclear Regulatory Commission
NPP	Nuclear Power Plants
PRA	Probabilistic Risk Assessment
PRM	Probabilistic Risk Management
RCS	Reactor Coolant System
RM	Risk Management
SAMG	Severe Accident Management Guideline
SNL	Sandia National Laboratories
TOP	Transient Over Pressure
UTOP	Unprotected Transient Over Power

EXECUTIVE SUMMARY

This report describes a severe accident management study for a small sodium reactor subjected to a 0.5g seismic event. A primary goal of this study was to analyze a beyond design basis accident in a dynamic event tree framework, exploring both the impact of uncertainties and human intervention, in order to provide operational insights to reduce potential for reactor damage. These objectives were accomplished. Another goal of this study was to use the insights from the accident analysis to create a Bayesian Network (BN) which can learn from the instrumented variables with the objective of inferring key states of the reactor. This objective was also accomplished. A third goal of this study was to use the BN to provide example inferences throughout the progression tree. This objective will be accomplished in follow-on research in FY15 under the DOE Advanced Reactor Concepts Work Package AT-15SN200304.

Key results

The overarching result from this report is that the small sodium fast reactor analyzed here-in is extremely robust to beyond design basis accidents. With the Direct Reactor Auxiliary Cooling System (DRACS) system working as designed, fuel melting is avoided in every accident progression tree branch. However, high sustained cladding temperatures can occur after a subsequent loss of flow due to excessive cold pool temperature rising above the primary pump trip set point (i.e., 525^{o}C). Two operator actions were considered to reduce the potential of cladding damage for this sequence: (1) modifying the DRACS system by inserting water to the air inlet and (2) overriding the primary pump trip set point.

The first accident management option is to increase the DRACS heat transfer rate by inserting water into the air inlet. This was modeled by increasing the DRACS heat transfer coefficient by an order of magnitude, an approximation which could obviously be improved by supplemental external calculations. This action staved off cladding failure for all accident progression branches except those involving the most unfavorable reactivity coefficients. From a correlated uncertainty study conducted separately from the accident progression tree analysis, this set of reactivity coefficients has an 8% chance of occurring.

Inserting water into the DRACS also introduces a potential failure mode for the DRACS because the operation of the system would exceed the design envelope of the DRACS. Failure of the DRACS was modeled by reducing the heat transfer coefficient by an order of magnitude, an approximation which again could be improved by supplemental external calculations. If the DRACS were to fail, fuel melting and cladding failure would be expected for every accident branch. The accident progression trees and the BN are not sufficiently developed to determine the optimal conditions for supplementing DRACS. Analyses of additional earthquake induced transients will be needed to assess the overall viability of this accident management method.

The second accident management option is to override the primary pump trip set point and allow the electromagnetic (EM) pumps to run until they overheat, in which case they would fail at the overheat temperature. It should be noted that a significant number of accident branches extended beyond the trip set point, but the inherent feedbacks in the reactor prevented subsequent pump failures. Endangering the pumps prevented the cladding failure end state while not opening the door to fuel failure, except for the branches where failed DRACS resulted in fuel failure.

In summary, enhancing DRACS has both greater upside and downside than overriding the EM pump set point when it comes to preservation of the core, but both can reduce core damage. The optimal strategy will depend on what state the operators infer (via the BN) the reactor to be in before they respond.

Future work

Bayesian Network Inferencing

The initial BN structure shows significant potential to support diagnosis and provide evidence-based insights into the value of different monitored parameters. Additional work is required before the BN model can be used to conduct activities related to inference on the variables in the model, including real-time decision support and further examination of SFR accident characteristics. Near-term BN development activities are focused on integrating the results from Section 5 into the model and subsequently performing inference on monitored parameters.

Additional efforts will also explore options for automating the quantification of the BN model using SAS4a results; this is a critical step in expanding the prototype model to include the extensive range of accident situations that must be represented in a severe accident management guideline (SAMG).

Expansion of the accident progression trees

Additional accident sequence scope will be added in future work, which will also lead to additional expansion of the BN model to demonstrate the ability for the BN model to reason across a larger accident suite. Multi-site risk issues researched conducted at Oak Ridge National Laboratory (ORNL) can be used to help inform prior uncertainties in the BN so that the impact of those uncertainties upon multi-site risk can be studies and those uncertainties and be prioritized for scrutiny in severe accident management strategies.

Decay heat removal experiments at Argonne National Laboratory (ANL) in both normal and degraded configurations will provide insights for developing branch point uncertainties in the discrete dynamic event tree (DDET) accident analyses. The DDET/BN decision support structure will be exercised to identify how these uncertainties could influence accident management. These results will help prioritize future experiments and tests. Future DDET/BN analyses will examine the impact of water ingress into air heat removal, which could inform the need for high fidelity models being developed at Idaho National Laboratory (INL). In the event that ANL test schedules slip past the point for incorporation into SNL DDET analyses, parametric sensitivity analyses will be performed to simulate the potential impact of phenomenological uncertainties related to the heat removal experiments, and experimental results would then be incorporated into future work.

1 INTRODUCTION

The advent of passive safety systems as a cornerstone of advanced reactor safety presents a revolutionary vision for reactor safety that will likely require the re-evaluation and adaptation of existing regulatory requirements and associated guidance for their implementation when compared to the existing commercial power reactors in the United States. See NUREG-1791 [1.1] and SECY-11-0098 [1.2] for a perspective on Nuclear Regulatory Commission (NRC) plans to address regulatory issues relevant to advanced reactor licensing. Therefore, the NRC anticipates that initially reactor vendors and utilities who seek advanced reactor Design Certifications, Manufacturing Licenses, and ultimately Combined Licenses will likely propose regulatory adaptations and apply for regulatory exemptions from certain licensing criteria established by the NRC.

Probabilistic Risk Assessment (PRA) will play a key role in establishing the safety case for regulatory exemptions and the acceptance of unique advanced reactor features. To do so, PRA tools, methods, and risk metrics that appropriately address the reliability and the uncertainties associated with the unique aspects of advanced reactor risk (e.g., passive safety system performance, alternative staffing options, and non-core-damage plant damage states) must be developed. The industry is expected to seek exemptions from NRC requirements regarding staffing, exclusion zones, etc. The methods being developed through this effort are expected to enhance the future justifications for those exemptions by further informing the static modeling results of passive systems.

In 2009 the NRC conducted a scoping Study [1.3] that set forth the NRC's expectations for advanced PRA methods that could be used to assess the safety case for advanced reactors. These requirements include reducing modeling simplifications (enhanced phenomenological modeling), improving consideration of human-system interactions, utilizing advances in computational capabilities, and characterizing uncertainty in analyses. Furthermore, the scoping study also calls for making the PRA process and PRA results more understandable. This improvement can enable better use of PRA results to facilitate decision making – a process called risk management (RM).

In previous work Sandia National Laboratories proposed an advanced PRA discrete dynamic event tree (DDET) method which can be used to support regulatory decisions regarding a generic iPWRs [1.4]. The method combines DDETs with plant simulations to provide comprehensive analysis of possible accident spaces. This meets the Scoping Study requirements for reducing modeling simplifications, characterization of uncertainty, and utilizing advanced computational capabilities. In the current work, we build upon the previous work to achieve better inclusion of human-system interactions and to improve the use of PRA information in the RM process.

1.1 Why Study Accident Management

Severe accidents are extremely rare in the nuclear power industry. However, as demonstrated by the Fukushima accident, rare events are not impossible events, and responding to these accidents can be extremely difficult. In the United States, NRC mandated Severe Accident Management Guidelines (SAMGs) serve as a critical resource that would help operating crews respond to severe accidents.

While not the reactor or accident sequence(s) analyzed in this report, the PRISM Probabilistic Risk Assessment [1.5] shows the impact of probabilistic uncertainty upon advanced reactor risks - a cliff-edge risk profile wherein the likelihoods of relatively small consequences (e.g., one to 10 latent fatality) are nearly the same as for moderate to high consequences (e.g., 10 to 1000 latent fatalities), with a significant and rapid drop in likelihood as the number of consequences increases to extremely high levels (see Figure 1.1). Advanced reactors tend to have lower overall safety risks than Light Water Reactors, but certain very low-probability events (e.g., extended loss of decay heat removal) could cause radiation release to increase from *de* minimis to significant levels. From a regulatory prospective, this behavior could be concerning because of the inherent uncertainty in calculating the risk. The result of this probabilistic uncertainty is that the likelihood of relatively large consequences (e.g., 100 to 1000 latent fatalities) can be undesirably high, causing a "cliff-edge" risk profile wherein the risk only starts to drop as the size of consequences moves up to extremely large values (e.g., 10,000 latent fatalities). Accident Management is a key tool that can be used to mitigate severe accidents whose probabilities of occurrence can be highly uncertain, and thus drive down the risk of the uncertainty of the cliff edge less significant (see Figure 1.1 [1.5]). The dotted line illustrates potential risk-reduction impact of accident management strategies. The line is for example only and does not represent any actual calculations involving accident management strategies. [1.5].

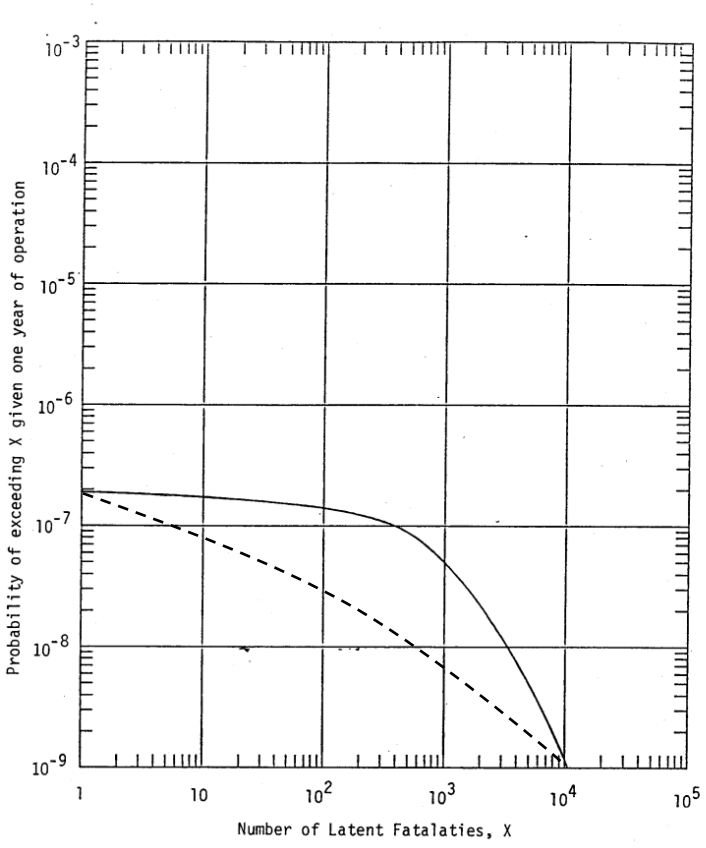

Figure 1.1 – Complementary Cumulative Probability Distribution of Latent Fatalities [1.5].

1.2 Approach

This report describes a risk-mitigation strategy for a generic small Sodium Fast Reactor (SFR) when faced with a large external event (i.e., a 0.5g earthquake). The annual occurrence probability of this event is estimated at $8x10^{-5}$, with an additional failure to SCRAM conditional probability of $1x10^{-3}$/large earthquake. Thus, most of the accidents analyzed in this report have an annual occurrence probability of $8x10^{-8}$ or less, which might place the scenarios in the beyond design basis or residual risk space based on a theoretical risk informed licensing framework. The Argonne National Lab (ANL) code SAS4A [1.6] is used to model SFR transient progression and the Bayesian Network program GeNIe [1.7] is used to model the relationship between reactor conditions and instrumented parameters, to enhance operators ability to diagnose the reactor condition from limited or uncertain information.

Note that because of incompatibilities with SNL's DDET code ADAPT [1.8] and SAS4A, the static accident progression trees were used instead of DDETs. This incompatibility is currently being resolved and future studies should use DDETs. For the purpose of this report, the two approaches are functionally equivalent because the accident progression tree used in this analysis is simple enough to ensure that all branch conditions are achieved. A more complex analysis, where branch conditions are dynamic enough to change the order of branches or remove branches altogether, would require SAS4A to be compatible with a DDET code like ADAPT.

Many mature SFR designs incorporate non-safety grade heat removal pathways which would be included in any PRA analysis; but the conceptual SFR chosen for this analysis has no such non-safety grade systems. Thus, they are not credited in this analysis.

1.3 Structure

The body of the report is broken into 4 sections:

- Chapter 2 describes the SAS4A model of a small SFR used to analyze the accident progression tree.
- Chapter 3 describes the operator actions and uncertainties which determine the branching within the dynamic event tree.
- Chapter 4 describes the structure of the Bayesian Network that will be used to reason through the accident progression tree.
- Chapter 5 describes the SAS4A output of the accident progression tree.

A supplemental report will be created exploring the reasoning capabilities of the Bayesian Network.

1.4 References

[1.1] J. Persensky et al., "Guidance for Assessing Exemption Requests from the Nuclear Power Plant Licensed Operator Staffing Requirements Specified in 10 CFR 50.54(m)," NUREG-1791, U.S. Nuclear Regulatory Commission, Washington, DC, July 2005.

[1.2] "Operator Staffing for Small or Multi-Module Nuclear Power Plant Facilities," SECY-11-0098, U.S. Nuclear Regulatory Commission, Washington, DC, July 2011.

[1.3] D. Helton (2009). "Scoping Study on Advancing Modeling Techniques for Level 2/3 PRA," U.S. Nuclear Regulatory Commission, May 2009. Available via the US NRC's ADAMS at accession no. ML091320454.

[1.4] K. M. Groth, M. R. Denman, J. N. Cardoni, T. A. Wheeler, "Proof of Principle Framework for Developing Risk-Informed Severe Accident Management Guidelines," SAND2013-8324, Sandia National Laboratories, Albuquerque NM, Sept. 2013.

[1.5] Hackford, N.E. (Ed.), 1986. "PRISM Preliminary safety information document," General Electric, Volume II, GEFR-00793.

[1.6] Argonne National Laboratory, Nuclear Engineering Division (2011) "The SAS4A/SASSYS-1 Safety Analysis Code System," ANL/NE-12/4, Argonne National Laboratory, Argonne, IL.

[1.7] M. J. Druzdzel. "SMILE: Structural modeling, inference, and learning engine and GeNIe: a development environment for graphical decision-theoretic models." In *Proceedings of American Association for Artificial Intelligence (AAAI-99)*, pages 902–903, 1999.

[1.8] D. Kunsman et al. "Development and application of the dynamic system doctor to nuclear reactor Probabilistic Risk Assessments." SAND2008-4746, Sandia National Laboratories, Albuquerque NM, 2008.

2 SAS4A AND SODIUM REACTOR MODEL

A reasonably detailed SAS4A [2.1] model of a 250 MWt, sodium-cooled, metal-fueled, small modular reactor is used for the calculations in Section 5 to provide realistic accident characteristics for the Bayesian network. The model was originally developed by Argonne National Laboratory (ANL). The SAS4A model includes representations of the core, primary coolant loop, intermediate coolant loop, balance of plant, and safety systems (e.g. direct reactor auxiliary cooling system [DRACS]). Model detail is higher for the core and primary coolant portions of the plant, since the code principally aims to ascertain the details of core channel thermal hydraulics and degradation/relocation of fuel and cladding. Congruently, the accident scenarios and problem scope are geared towards the simulation of core phenomena, as opposed to assessing wider plant and containment responses akin to source-term analyses.

The SAS4A model is used in this work primarily to evaluate unprotected transient overpower scenarios in conjunction with other boundary conditions such as operator actions and equipment failures. The reactivity insertion is chosen to be the result of a large earthquake the drives control rod oscillations and core "sloshing" (i.e. radial movement of fuel assemblies). The original ANL model was already capable of simulating reactivity insertion scenarios (e.g. rod withdrawal) and unprotected loss of flow accidents. Hence, SNL has made simple modifications to permit the simulation of different reactivity insertion functions and magnitudes, assumed operator actions, and dynamic equipment failures such as thermal pump failure.

Section 2.1 provides a brief description of the SAS4A code and the input model used in this work–its physical representations of the core and RCS are discussed as are some pertinent inputs. The majority of the model modifications by SNL is limited to boundary condition and control system inputs, which are discussed in Section 2.2.

2.1 Physical Plant Representation

A very cursory overview of the SAS4A code is described in Section 2.1.1 to provide adequate context for the accident scenarios investigated in this work. More in-depth descriptions of the physics and models used by SAS4A can be found in the appropriate theory manuals [2.1]. Section 2.1.2 provides an overview of the spatial nodalization of the model and discusses some key inputs relevant to transient overpower scenarios.

2.1.1 Modeling Approach

SAS4A is a system-level code developed by ANL that is capable of simulating LMR thermal-hydraulics (core and RCS), neutronics, and LMR accident phenomena. Core thermal-hydraulics and fuel/cladding degradation are treated using a channel approach: A few channels may be used to represent comparable regions of the core (e.g., inner and outer core, peak limiting channel, reflector, etc.), the assumption being the channel sufficiently represents its respective region. Alternatively, the user can input many channels (e.g. 50+) to discretize the core. Each channel is comprised of several axial nodes, usually 20 or more, over which the thermo-fluid equations are resolved assuming one-dimensional flow. The channel can represent a single fuel element and surrounding coolant or several rods in a fuel bundle. Fuel and cladding are radially discretized

into several nodes for calculations of heat transfer and material degradation. An illustration of a SAS4A channel and its mesh schemes are shown in Figure 2.1.

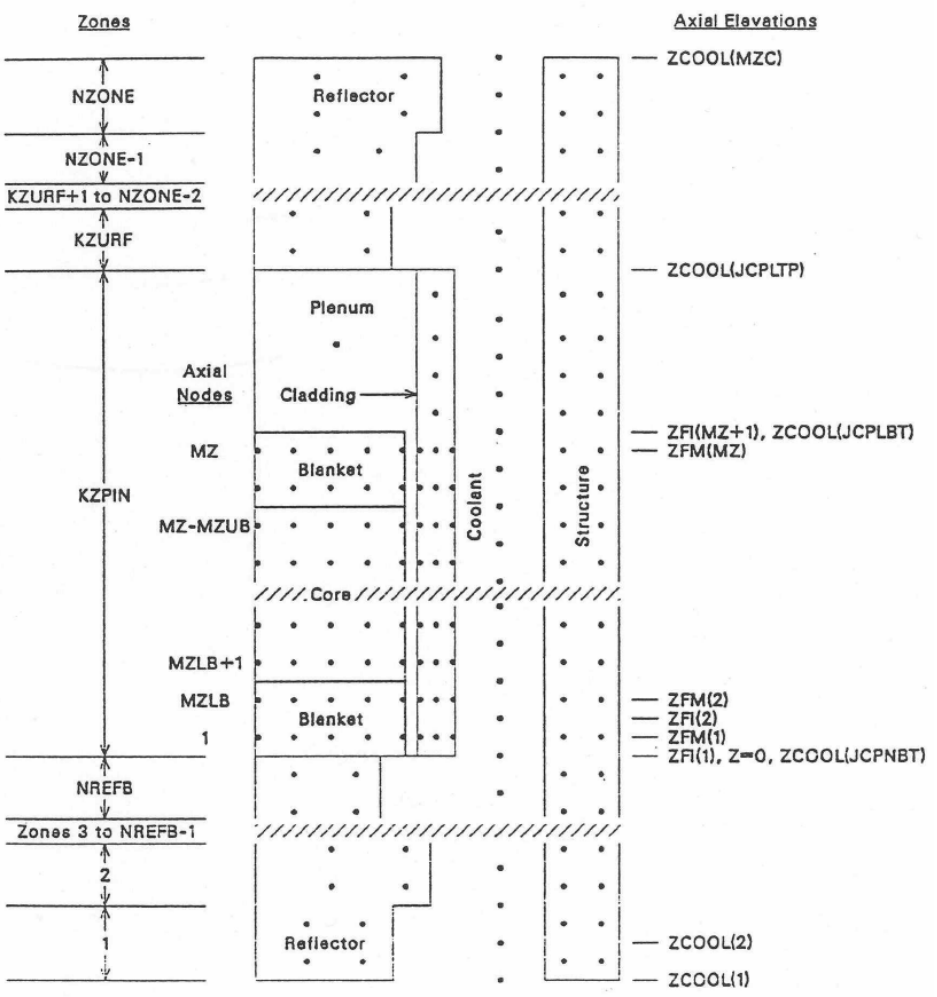

Figure 2.1 – Illustration of SAS4A channel (dots represent the radial/axial mesh) [2.1].

SAS4A uses distinct thermal-hydraulic formulations for the core channels and the plant; hence the core thermal-hydraulics is oriented towards channel flow physics and includes a detailed sodium boiling model (multiple bubble slug ejection [2.1]). Plant thermal-hydraulics is treated in the PRIMAR4 module of SAS4A and is conceptually similar to LWR safety codes in its use of volumes, flow paths, and components in a one-dimensional formulation. Further, the thermal-hydraulic behavior of the water-side portion of the plant[1], excluding the steam generators, has dedicated models in the Balance of Plant module of SAS4A. The steam generators are treated with a simpler model that neglects momentum effects and couples explicitly to the Balance of Plant model. Many severe accident scenarios for SFRs, such as the unprotected transient overpower (UTOP) scenarios considered in this work, are not predominantly concerned with the steam generators and balance of plant components, but are instead more concerned on power and flow transients of the primary and intermediate coolant loops.

[1] The SFR model used in this work actually has a CO_2 plant. The 'steam generators' in this model are Na/CO_2 heat exchangers between the intermediate sodium loop and the CO_2 working fluid.

For severe accident scenarios, SAS4A calculates fuel and cladding heatup, liquefaction (including eutectic reactions), material relocation, and cladding failure. Debris momentum, coolant interaction, and refreezing are treated in addition to reactivity feedback effects due to material relocation; relocation feedback is notionally accounted for by pre-generating a set of reactivity coefficients for fuel and cladding relocation in each channel and axial node, which SAS4A subsequently uses to determine reactivity magnitudes to insert into its point kinetics equations (nodal diffusion kinetics may optionally be used with coupling to other codes). This approach is very similar to the treatment of the usual SFR feedback mechanisms. For instance, the user can specify sets of reactivity feedback information for fuel Doppler feedback, axial fuel/cladding expansion, radial core expansion, and coolant density. Such information can be input for each channel at each axial node.

In contrast to many LWR severe accident and source term codes, SAS4A does not simulate gross core destruction and material relocation such as radial debris relocation between failed channels, core slumping, and subsequent vessel/containment failure. The extent of its fuel relocation can be inferred from the TREAT experiments that SAS4A is benchmarked to: Fuel can melt and expand axially into the gas plenum within the cladding (thus driving negative feedback), or it can burst through a cladding failure and relocate up or down in the channel–it may then induce further failures in other channels, via further coolant boiling and positive feedback, or terminate the transient due to the negative feedback that follows reduced gross fuel density in the core and increased leakage. Of course, several other phenomena are involved in this process and treated in an integrated fashion, the details of which can be found in the SAS4A manuals [2.1].

2.1.2 SAS4A Model Nodalization and Key Inputs

The core region is modeled using five channels. Three channels are used for the bulk of the core that represent the inner core, middle core, and outer core. Of these three channels, the inner core channel is the most thermally limiting–its peak material and coolant temperatures generally exceed those in the other main channels for most accident scenarios. In addition to these main channels, a fourth channel is used to represent the non-fueled reflector regions, and a fifth channel represents the most thermally-limited region of the core in terms of peak power to flow ratio. Thus, the core region is represented by five total channels. Each channel actually represents several fuel assemblies that exhibit comparable power and flow characteristics. A summary of the SAS4A model is provided by Table 2.1.

Table 2.1. Nodalization summary of SAS4A SFR model.

Parameter	Value
Number of channels	5
Number of axial nodes for fuel mesh	22
Number of axial blanket nodes above fuel	2
Number of axial nodes for coolant mesh	28
Number of radial nodes for fuel	10
Number of radial nodes for cladding	3
Number of compressible volumes in plant	10

There are some key inputs in the SAS4A model pertinent to the UTOP scenarios for this work. Two extra nodes are incorporated above the active fuel region to allow PINACLE to initiate in-pin fuel motion. These extra nodes are treated as blanket nodes with very low power; this allows for the simulation of severe accident scenarios where melted fuel may expand into the upper plenum region of the fuel element. For radial expansion of the core, the inlet coolant temperature is used in conjunction with the simple radial expansion model. Axial expansion of the fuel considers both thermal and force effects, and the propagation of axial fuel failures (if any) are treated mechanistically by the PLUTO and LEVITATE modules. The detailed feedback models in SAS4A are specified in the model to determine reactivity feedback for the 6-group point kinetic calculations.

The fuel material in the SAS4A model is a U-Pu-Zr metal alloy. Its solidus and liquidus temperatures are taken to be 1353 K and 1588 K, respectively. DEFORM5 is used to simulate fuel-cladding eutectics and cladding wastage. Eutectic reaction rate is determined by correlations that are functions of temperature only. Further work may investigate alternative correlations that include other parameters such as burnup. DEFORM5 also calculates cladding stress/strain and rupture time based on the thinning of the cladding due to eutectics and the pressure inside the fuel element. More detailed models of the pre-failure behavior of fuel and cladding are available in FPIN2, but the DEFORM5 models are sufficient to provide reasonable estimates of cladding wastage and failure for the Bayesian models.

2.2 Inputs for Accident Scenario and Progression

Most of the SNL modifications made to the original (ANL) SAS4A model are limited to boundary condition and control system inputs. These modifications are necessary to support the simulation of new accident scenarios in this work.

2.2.1 Boundary Conditions

The accident scenarios investigated in this work are earthquake-induced UTOPs that involve axial and radial oscillations of the reactor, which are represented as sinusoidal functions of reactivity insertion. The axial oscillations characterize movement of the control rods. Therefore, control rod expansion feedback is neglected. This assumption is somewhat conservative since the controls rods tend to expand into the core as temperatures increase, thereby inserting negative reactivity; some thermal expansion into the core might still occur even with the rods oscillating.

All accident scenarios assume a loss of balance of plant simultaneous with the earthquake reactivity insertion begins (near t=0). The DRACS is treated as functional, but the tube-to-air heat transfer coefficient for the air dump heat exchanger (ADHX) is variable (i.e. a DDET branch parameter) in the event tree calculations in Section 5.2. The pump torque and external reactivity tables are disabled in the SAS4A input to support dynamic pump trips and various reactivity insertions (e.g. earthquake and/or scram); instead, pump torque and external reactivity is linked to the control system input. Finally, pump coast-down is assumed constant in all scenarios with a 10 s halving time. Coast-down of the EM pumps is an important safety feature for power and flow transients.

A summary of the boundary conditions in the SAS4A input model is listed below:

- Control rod expansion feedback is neglected.
- BOP is lost after t=0
- DRACS is fully functional
    - Tube-to-air heat transfer coefficient for air dump heat exchanger is variable
- Pump controls are linked to control system
- Reactivity insertion is linked to control system
- Pump coast-down is left at nominal value of 10 sec halving time

2.2.2 Control System Input Additions

Several additions are made to the control system inputs in the SAS4A model that are necessary to simulate the UTOP scenarios driven by sinusoidal (earthquake-driven) reactivity insertions. Control system inputs are specified for two, superimposed, sinusoidal functions with distinct periods and magnitudes. The reactivity functions have time-dependent, linear multipliers applied to their magnitudes to represent gradual dampening of the earthquake. A large negative reactivity (e.g. -14$) can also be inserted at different rates to represent normal shutdown and scram under degraded conditions that would cause slower insertion of the control rods. Control system inputs are specified that allow scram can occur at a specific time or based on various signatures such as excessive power or temperature. Finally, the new input for control system allows for dynamic pump operation such as throttling by the operators and pump trip due to high temperature in the cold pool.

A summary of the control system modifications in the SAS4A input model is listed below:

- Two superimposed, sinusoidal reactivity functions
- Sine functions have different peak magnitudes and frequencies
- Sine functions have time-dependent dampening multipliers
    - Multipliers input via tables
- Variable operator scram based on simulation time
    - Mimic operator scram
    - Shuts down reactor via large negative reactivity insertion
    - Variable control rod insertion rates
- Variable pump trip based on:
    - Cold pool temperature
        - Thermal failure temperature and operator action temperature
    - Flow rate
    - Simulation time (i.e. to mimic operator pump trip)
- Two pump ‘throttling’ functions that are functions of time
    - Pump torque multiplier before trip event: represents operator throttling
    - Pump torque multiplier after trip event: represents partial pump failures (i.e. 2/4)

2.2.3 Seismic Events

The initiating event of this study was a beyond design basis seismic event. The reactivity impact of seismic induced motion on control rod positions and sodium sloshing was taken from the ALMR PRA [2.2]. For licensing applications, these reactivity effects would have to be calculated directly for a given sodium reactor. The assumed reactivity amplitudes for various earthquakes

are seen in Table 2.2. Control Rods (CR) oscillate with the vessel head (reactor building), while Core Sloshing (CS) will peak at the same time as CR but will dampen quicker.

Table 2.2 – Example Reactivity Insertions for Various Theoretical Sceismic Events

Size (g)	Freq. (yr^{-1})	CR ($)	CS ($)
0.3	$1x10^{-4}$	0.163	0.228
0.5	$2x10^{-5}$	0.278	0.380
0.7	$6x10^{-7}$	0.548	0.418

The reactivity amplitudes do not extend indefinitely; they rise and then dampen over time. For large earthquake, studies have shown that the majority of earthquake effects can extend for 20-25 seconds (see Figure 2.2). The rise and fall in reactivity amplitude from the maximum value is approximated by linearly interpolating Table 2.3.

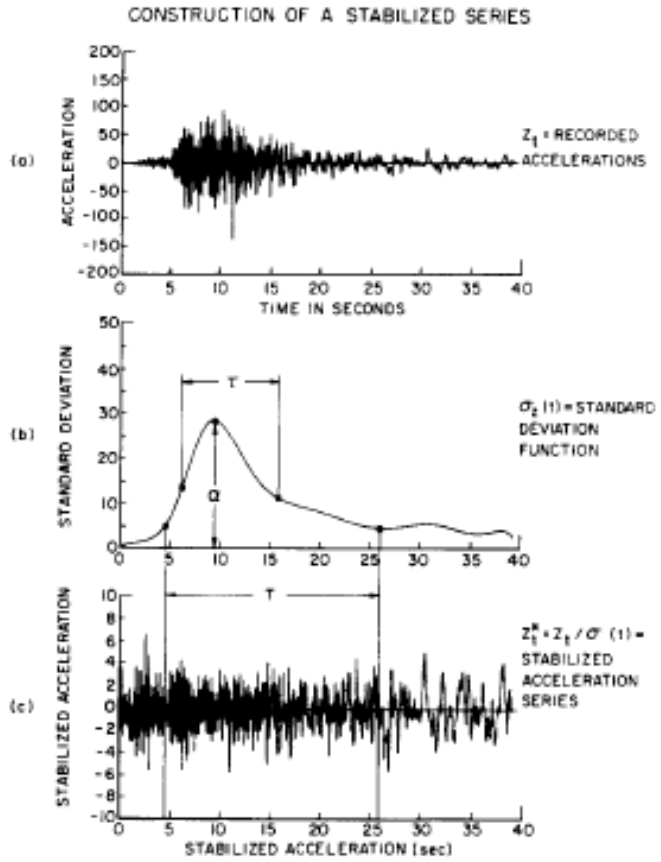

Figure 2.2 – Example Large Earthquake Spectrum [2.2]

Table 2.3 – Assumed Reactivity Dampening Table for 0.5g Seismic Event

Time (s)	CR Amp.	CS Amp.
0	0	0
1	0.1	0.1
3	0.15	0.15
5	0.5	0.5
8	1	1
15	0.9	0.9
20	0.8	0.6
25	0.5	0.1
50	0.1	0
100	0	0

2.3 References

[2.1] Argonne National Laboratory, Nuclear Engineering Division (2011) "The SAS4A/SASSYS-1 Safety Analysis Code System," ANL/NE-12/4, Argonne National Laboratory, Argonne, IL.

[2.2] K. A. El-Sheikh, "Probabilistic risk assessment of the advanced liquid metal reactor," GE Nuclear Energy. GEFR-00873, 1994.

[2.3] A. S. Cakmak, R. I. Sherif, and G. Ellis, "Modelling Earthquake ground motions in California using parametric time series modeling," Soil Dynamics and Earthquake Engineering, Vol. 4, No. 3, pg. 124-131, 1985.

3 OVERVIEW OF THE ACCIDENT PROGRESSION TREE

This section will briefly describe the branch parameters used to define the accident response/decision tree which will be used to train the Bayesian Network. In Section 3.1, the branch parameter probabilities will be defined. In Section 3.2, the decision tree will be presented.

3.1 Branch Parameters

The branch parameters can be broken into two groups: operator action (with associated uncertainties), inherent reactivity related uncertainties, and high temperature EM pump performance uncertainties.

3.1.1 Operator Actions

This section will describe the two operator actions incorporated in the accident progression tree: (1) enhanced DRACS performance (likely by pouring water into the air intake to improve heat transfer) and overriding the EM Pump high temperature trip to delay a loss of flow at high temperatures.

3.1.1.1 DRACS Enhancements

The DRACS is a passive air cooled heat removal system. It is designed to reject heat across a wide range of accidents, but no system can be designed to function successfully over every conceivable accident. Thus, if the operators determine that a given accident may exceed the design capability of the DRACS those operators may wish to increase heat transfer in the DRACS by inserting water into the air intake. It is assumed that the water will increase the heat transfer in the DRACS by an order of magnitude, but this assumption may be improved by passive heat removal studies currently being conducted at ANL [3.1].

It is possible that the DRACS piping cannot withstand thermal stresses induced by the addition of water. Thus, if the operators enhance the DRACS it is assumed that there is a 10% chance that the system will fail and the heat removal from the DRACS will drop by an order of magnitude. Table 3.1 reviews the potential DRACS branches.

Due to code limitations, it is assumed that the operators will enhance the DRACS at the initiation of the earthquake. This is a non-conservative assumption that will require a code revision to address.

Table 3.1 – DRACS Operation Actions

Enhance DRACS?	Successful?	Prob. Given Action	Relative Heat Transfer to Design
No	N/A	N/A	1.0
Yes	Yes	0.9	10.0
Yes	No	0.1	0.1

3.1.1.2 EM Pump Interfaces

In this analysis, operators are allowed to interface with the primary pumps in two ways:

1. Increase pump torque by 50% seconds into the accident sequence and
2. Override the thermal trip of the EM pumps.

One of the primary drivers of fuel damage during a transient is a power to flow mismatch. Since the seismic event imitates a reactivity insertion, operators may wish to increase coolant flow rates in the system by increasing pump torque. This action may not be beneficial because increasing pump torque will cool the fuel and dilute some of the inherent feedbacks associated with a hotter core. These actions are summarized in Table 3.2.

Table 3.2 – EM Pump Operation Actions - Torque

Increase Pump Torque	Result
No	All pumps remain at their nominal torque
Yes	All pumps increase torque by 50%

The EM pumps are designed with a thermal shutdown at 525^{o}C to protect the pumps from overheating. In the case of a beyond design basis accident, the operators may choose to sacrifice the EM pump in order to reduce the potential for fuel damage. These actions are summarized in Table 3.3.

Table 3.3 – EM Pump Operation Actions – Thermal Trip

Override Thermal Shutdown?	Result
No	All pumps coast-down at a cold pool temperature of 525^{o}C.
Yes	All pumps coast down given their thermal failure criteria.

3.1.2 Reactivity Coefficient Uncertainties

During an unprotected transient, SFRs rely on reactivity feedbacks to provide for inherent safety. During beyond design basis events, these accidents have significant uncertainties as geometries may change and feedbacks extend beyond the design envelope of the reactor. Table 3.4 shows the 1-sigma estimates of a standard normal distribution for various reactivity feedbacks.

3.1.2.1 Correlated Uncertainty Analysis

Not all of the uncertainties in Table 3.4 were feasible to study. Additionally, it is reasonable to assume that some correlation structure exists between the feedbacks. For example, a higher or lower energy (e.g. harder or softer) neutron spectrum than expected may bias all the feedback mechanisms in a consistent manner. Thus, a correlation coefficient of 0.5 was assumed to allow for such impacts.

Table 3.4 – SFR Reactivity Coefficient Uncertainties [3.2]

Uncertainty[a] Assignments in Reactivity Coefficients
Used in ANL Risk Assessments of Advanced LMR Concepts

Reactivity Feedback Mechanism	Metal	Oxide
Doppler	20%	15%
Na Density	20	20
Fuel Axial Expansion/Contraction	30	25
-- neutronic	20	15
-- thermo-mechanical	20	20
Net radial expansion (P/F >0.8) (including bowing)	20	20
Neutronic	15	15
Thermal hydraulic	10	10
Structural	10	10
(P/F <0.8)	50	50
Neutronic	15	15
Thermal hydraulic	15	15
Structural	50	50
Control Rod Expansion	20	20
-- neutronic	10	10
-- thermal-hydraulic	<20	<20
Pre-clad failure, in-pin, molten fuel relocation	Not evaluated	Not evaluated
Vessel Axial Expansion	Not evaluated	Not evaluated
Core Support Structure Expansion	Not evaluated	Not evaluated

a Values shown represent 1σ deviations from the mean of a normal distribution expressed as percentages of the best estimate reactivity coefficient. "Sub-effect" contributions are statistically combined to develop the five major short term reactivity feedback uncertainties, which are rounded to the nearest 5%.

The accident progression tree analysis requires discrete combinations of reactivity coefficients, likely on the order of 3-4 combinations which would be representative of the spectrum of accident responses. In order to accomplish this goal, the reactivity coefficient distributions were sampled (using the 1-sgma uncertainty values in Table 3.5 and run in a representative sequence (i.e., 0.5g earthquake, failure to SCRAM, pumps never experience high temperature failure). The hot channel temperature results from this study are shown in Figure 3.1.

Table 3.5 – Distribution Sampled for the Correlated Uncertainty Study (ρ = 0.5)

Feedback	Uncertainty
Sodium Density	20%
Doppler	20%
Radial Expansion	20%
Axial Expansion	30%

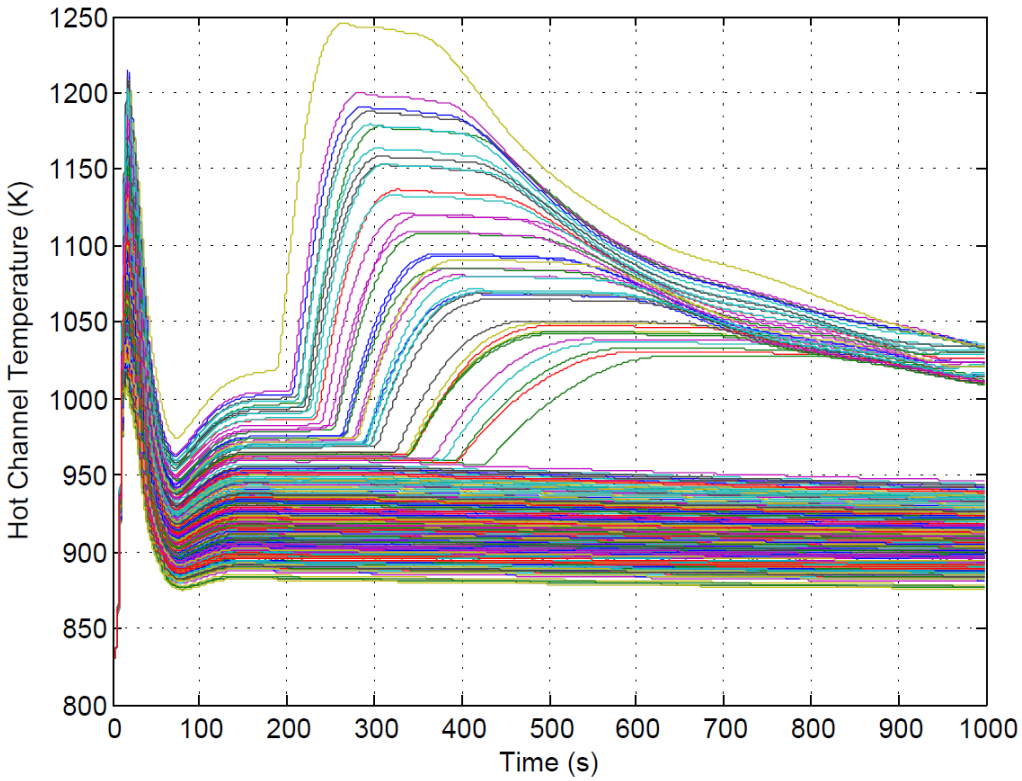

Figure 3.1 – Time histories from the Correlated Uncertainty Analysis

3.1.2.2 Gaussian Clustering

After the correlated Monte Carlo (MC) analysis, 500 sets of reactivity coefficients produced 500 time histories, of which a small number of sets of reactivity coefficients are needed. In general, SFR accident response attempts to minimize both the peak and average temperatures in the system. High peak temperature may lead to sodium boiling, which can divert the accident into a new operating regime due to the sodium void coefficient. High average temperatures can lead to time at temperature failures of structures or components. Plotting the peak verses average hot channel temperatures for the correlated MC simulation produces the data points in Figure 3.2. Three regimes appear to exist:

1. Robust Regime – Low peak and average system temperatures with a relatively small variance slope.
2. Nominal Regime – Extension of the robust regime but with a slightly higher variance in the slope.
3. Sub-optimal Regime – Reduced slope compared to the robust and nominal regimes.

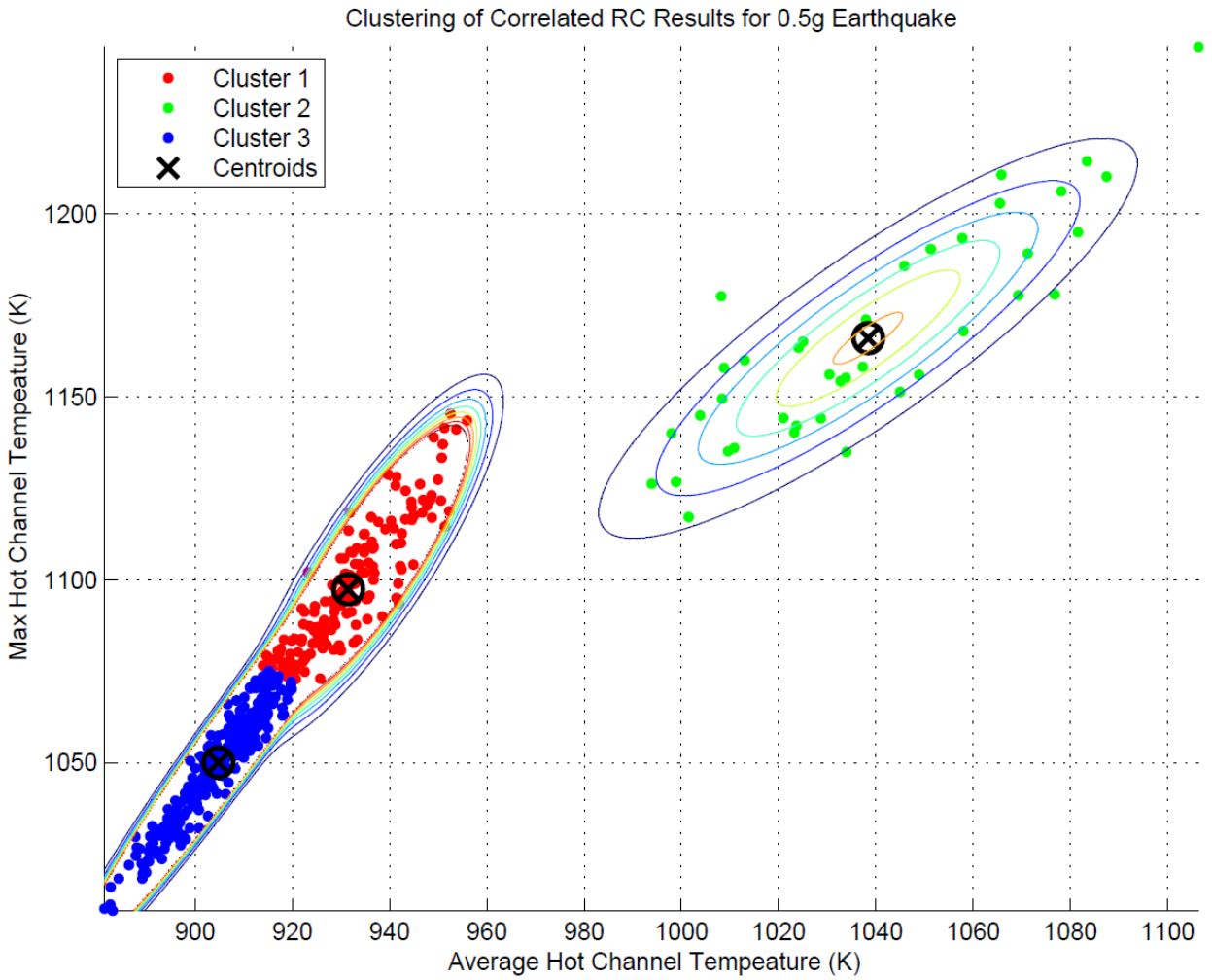

Figure 3.2 – Gaussian Clustering results for the Correlated Uncertainty Analysis

Using MATLAB's Gaussian Clustering algorithm [3.3], the three regimes were segmented into three bivariate Gaussian clusters. The MC sample nearest to the centroid of the cluster was selected to represent the overall behavior of the cluster. The weight of each cluster is extracted from the Gaussian clustering algorithm and is roughly related to the fraction of the MC samples within each cluster. The results can be seen in Table 3.6.

3.1.3 High Temperature EM Pump Performance

High temperature performance and reliability of large EM pumps have not been characterized in the open literature, and most of the close literature testing data conducted at ETEC has been lost in the resulting decade of inactivity for SFRs in America. Even with a lack of directly applicable studies on high temperature large EMP performance, four indirect sources of information are utilized to create proof of principle temperature dependent hazard function, $\lambda(T)$, for EM Pumps:

Table 3.6 – Clustering Results

Reactivity group ID	Weight	Coefficient Multipliers
1	0.21	Doppler = 0.81 Sodium Density = 0.83 Axial Expansion = 0.78 Radial Expansion = 1.06
2	0.71	Doppler = 0.86 Sodium Density = 0.99 Axial Expansion = 1.09 Radial Expansion = 1.21
3	0.08	Doppler = 1.04 Sodium Density = 1.34 Axial Expansion = 1.45 Radial Expansion = 1.16

1. An Idaho National Engineering Laboratory summary report on the CREDO database which provides operating temperature (675 K) reliability estimates (i.e., Failure to Run - $1x10^{-5}$/hr. with an error factor (EF) of 10) [3.4].
2. Expert elicitation that EM pumps quickly degraded above the EM pump trip set-point due to insulation degradation and subsequent damage to the magnets and other electrical components [3.5].
3. The reactor pump trip point of 525^{o}C, which is theoretically designed to trip with some margin before significant pump degradation [3.6].
4. A variety of studies which have shown that may components degrade at high temperature with an Arrhenius (exponential) relationship.

From these four observations, three distributions are created to fit potential Arrhenius degradation curves to the reliability of EMPs at different temperatures (see Table 3.7). The nominal performance distribution is pulled directly from the INEL report in the first bullet. The temperature at which a low reliability value is assumed is distributed between 825K and 875K. The lower and upper bounds are assigned at 25K and 75K above the pump trip set-point through engineering judgment. The probability density in this range was assigned to be a beta distribution with shape parameters $\alpha=2$ and $\beta=2$ to allow for a diffuse distribution with a central tendency. The high temperature depredated performance is assumed to have a high failure rate (approximately 1/hr.) with an error factor around that failure rate of 7.5, which is slightly narrower than the low temperature failure rate due to higher certainty in the expected failure modes. The low temperature and high temperature failure rates are assumed to be rank correlated because any defects that would cause a higher hazard rate at low temperatures would likely be amplified at high temperatures (e.g., poor insulation quality).

Table 3.7 - Distributions used to fit the Arrhenius hazard rate curves

Parameter	Distribution	Notes
Low Temperature Hazard Rate	LN(mean=1x10^{-5}/hr. , EF=10)	$\lambda(T = 675K)$, Rank correlated with $\lambda(T = T_{Hot})$
High Temperature Hazard Rate	LN(mean=1/hr. , EF=7.5)	$\lambda(T = T_{HOT})$, Rank correlated with $\lambda(T = 675K)$
High Temperature Estimate	$825K + \mathrm{B}(\alpha = 2, \beta = 2) * 50K$	Engineering judgment, no correlations

The Arrhenius relationship used to calculate $\lambda(T)$ takes the form of Eq. 1. A and B are shape parameters that can be fit using samples from Table 3.7. The Horsetails from a Monte Carlo sampling and fitting scheme can be seen in Figure 3.3. The Horsetails that most closely resemble[2] the 25th and 75th percentiles of the horse tails, along with the mean of the horse tail curves, shown in Figure 3.3 can be seen in Figure 3.4.

$$\lambda(T) = A * exp(B * T) \tag{1}$$

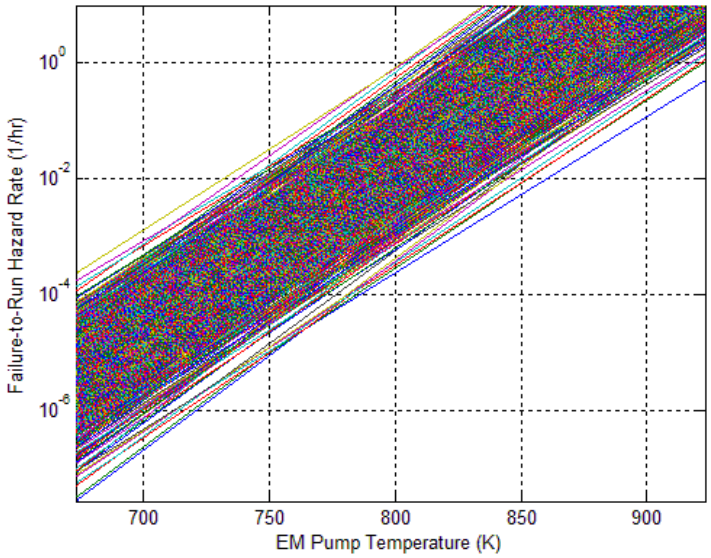

Figure 3.3 - Horsetail Arrhenius hazards curves for temperature dependent EM pump performance.

[2] Note: Because the epistemic samples overlap, the percentile estimates may correspond to a piecewise hybrid of multiple epistemic curves. Because a given epistemic curve represents a potential reality, it is inappropriate to use a hybrid curve in a given uncertainty set. Thus, the epistemic curves which most closely align with a given percentile curve is used for the subsequent SAS4A analysis.

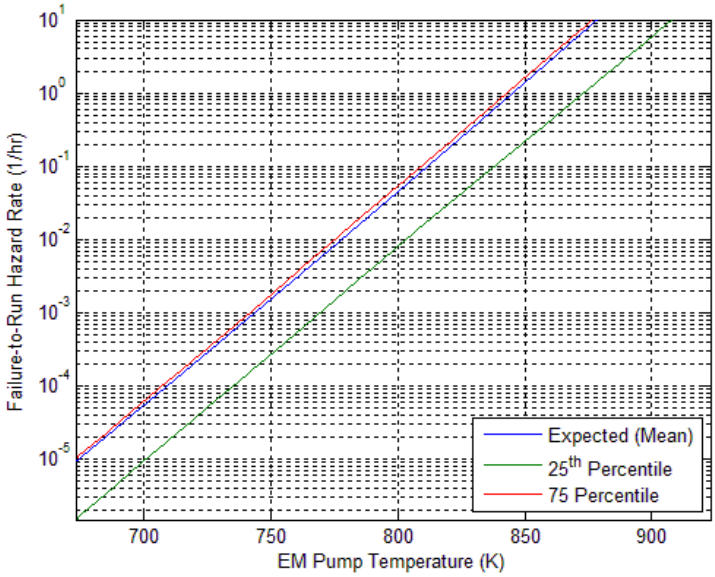

Figure 3.4 – Mean, 25th and 75th percentile estimates of the Arrhenius hazard curves from Figure 3.3.

Figure 3.5 shows a histogram which approximates the joint probability distribution for the Arrhenius shape parameters A and B. These shape parameters form the basis of the horsetails in Figure 3.3. The A and B pairs which most closely matches the 25th and 75th percentile estimates in Figure 3.4 can be seen in Table 3.8.

Table 3.8 - Shape parameters pairs which most closely match the 25th and 75th percentile estimates in Figure 3.4.

Percentile	A (1/hr.)	B (1/K)
25th	2.0486×10^{-26}	1.4541×10^{-26}
75th	0.0674	0.0668

In order transform the variable hazard rate curves into cumulative failure distributions [3.7] from which failure timings can be estimated, the reader should remember that definition of the hazard rate (Eq. 2) is the conditional probability that a component will fail in the following dt given that it survived until the current time. Specifically, the hazard rate is the probability of failing at a given time ($f(t)dt$) divided by the probability that the component survived until time t, ($S(t)$).

$$\lambda(T) = \frac{f(t)}{S(t)} \tag{2}$$

where:

$$1 - S(t) = F(t) = \int_0^t f(s)ds \tag{3}$$

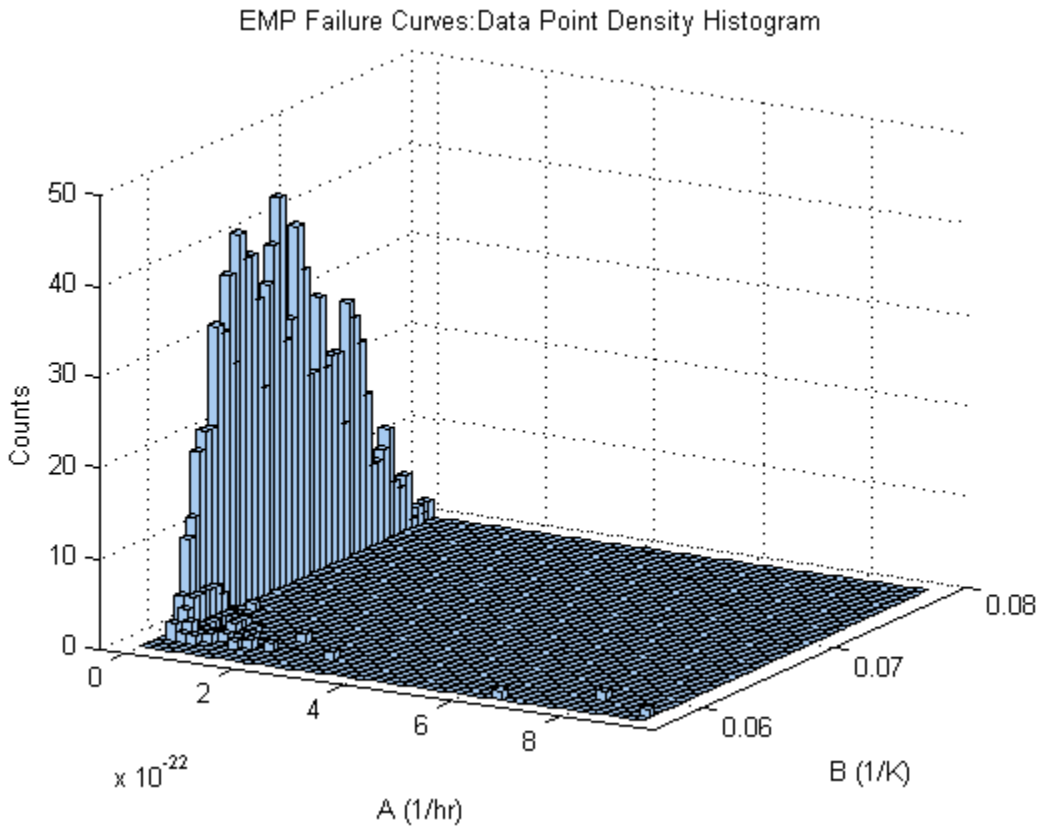

Figure 3.5 – Histogram of shape parameter pairs (A,B) from the Arrhenius hazard curves.

by integrating Eq. 2 from zero to one, assuming the pumps were functioning at t=0 and rearranging the terms, the cumulative failure probability $F(t)$ can be calculated through Eq. 4.

$$F(t) = 1 - \exp\left(\int_0^t \lambda(s|T)ds\right) \tag{4}$$

Converting the analytic integral into a numeric integral, the cumulative failure probability is calculated in Eq. 5, where a summation of the hazard function evaluated at the cold pool temperature in time step i is multiplied by the width of time step i determines the probability that the EM pump failed before time step i. The effective 25th and 75th percentile hazard curve estimates are combined with a theoretical 1K/s cold pool temperature ramp to calculate the corresponding cumulative failure curves in Figure 3.6.

$$F(t) = 1 - \exp\left(\sum_{i=0}^{N} \lambda(t|T_i) * \Delta t_i\right) \tag{5}$$

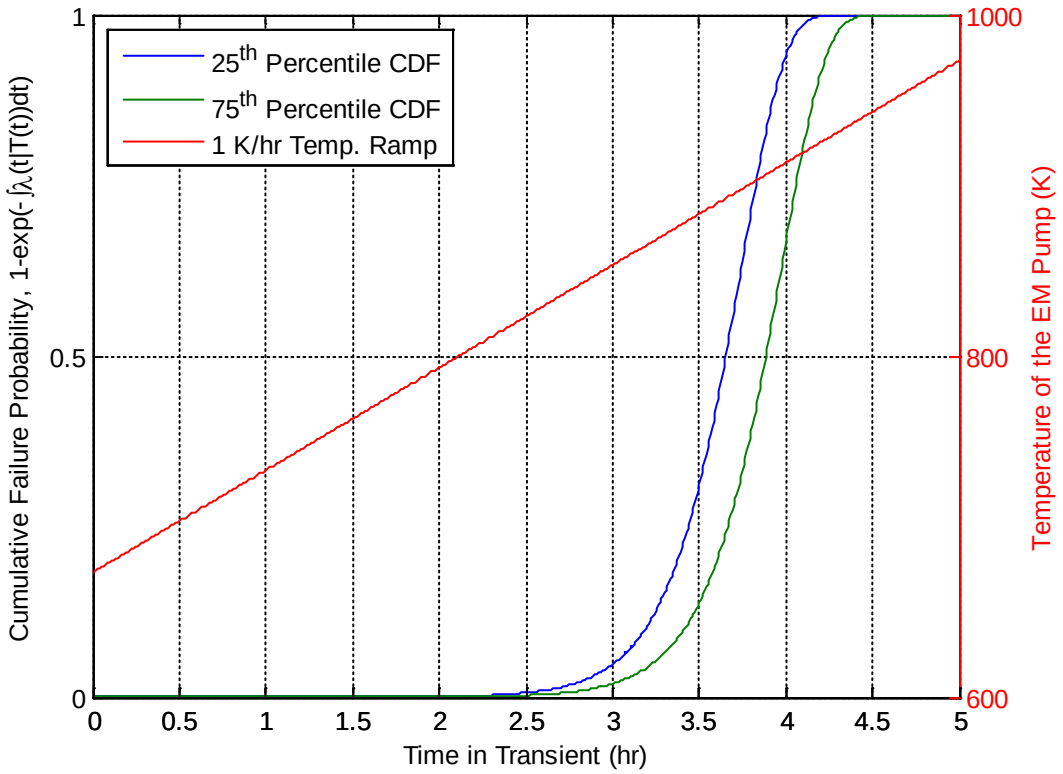

Figure 3.6 – Cumulative failure probabilities assuming the shape parameters in Table 2 and a 1K/s cold pool temperature ramp.

Because most of the variability in EMP timing of failure is due to aleatory, not epistemic (surprisingly), uncertainty, the aleatory uncertainty will be broken into two bins also represented by the 25th and 75th percentiles. For a four EMP system, if the EMP failures were independent, the probability of failing zero, one, two, three or all EMPs at the first failure point (i.e., 25th percentile) could be calculated from the binomial distribution of four trials. The conditional probability of all pumps failing given they did not fail at the 25th percentile is 1.0, because the upper bin accounts for temperatures which cause all pumps to fail. The branch probabilities for the independent failure case can be seen in Table 3.9.

Table 3.9 – Branch probabilities for EMP failure at the 25th and 75th percentiles given EMP failures at the 25th percentile are independent.

Case	0 Pumps Fail	1 Pumps Fail	2 Pumps Fail	3 Pumps Fail	4 Pumps Fail
Independent 25th Percentile	0.0625	0.25	0.3750	0.25	0.0625
Independent 75th Percentile	0	0	0	0	1

The ALMR PRA recognizes that flow instabilities from the failure of one EM pump may introduce a common cause failure mode which fails all of the remaining pumps. Thus, Table 3 is

modified so that 10% of the failure probability for 1-3 failed pumps is transferred into 4 pumps fail. Those branch probabilities are seen in Table 3.10.

Table 3.10 – Branch probabilities for EMP failure at the 25th and 75th percentiles given EMP failures at the 25th percentile are independent.

Case	0 Pumps Fail	1 Pumps Fail	2 Pumps Fail	3 Pumps Fail	4 Pumps Fail
Independent 25th Percentile	0.0625	0.225	0.3375	0.225	0.15
Independent 75th Percentile	0	0	0	0	1

To prevent combinatorial explosion within the dynamic event tree, the 1 and 3 pump failures were removed. These results can be seen in Table 3.11.

Table 3.11 – Branch probabilities for EMP failure at the 25th and 75th percentiles given EMP failures at the 25th percentile are independent.

Case	0 Pumps Fail	2 Pumps Fail	4 Pumps Fail
Independent 25th Percentile	0.1875	0.625	0.1875
Independent 75th Percentile	0	0	1

The ALMR PRA recognizes that flow instabilities from the failure of one EM pump may introduce a common cause failure mode which fails all of the remaining pumps. Thus, Table 3 is modified so that 10% of the failure probability for 1-3 failed pumps is transferred into 4 pumps fail. Those branch probabilities are seen in Table 3.12.

Table 3.12 – Branch probabilities for EMP failure at the 25th and 75th percentiles given EMP failures at the 25th percentile are independent.

Case	0 Pumps Fail	2 Pumps Fail	4 Pumps Fail
Independent 25th Percentile	0.169	0.563	0.268
Independent 75th Percentile	0	0	1

3.1.4 SCRAM Reliability

The probability of control rod drop after release for a 0.5g or greater earthquake is $1x10^{-3}$/demand. If the control rods do not insert, there is a follow-on operator action where control rod drive motors force the control rods into the core. This operator action has a failure probably of $1x10^{-4}$/demand (which may be optimistic for a scenario in which the control rod is physically jammed). While this action is not included in the evaluated scenario, any such consideration would reduce the sequence probability even further.

3.2 Event / Decision Tree

The full decision tree for the set of transients analyzed in this report is shown in Figure 3.7. The BN reasoning structure must be able to decipher between earthquake and non-earthquake conditions, thus the decision tree must include a non-earthquake portion with enough branches to demonstrate to the BN that there is variability to a normal accident sequence. The non-earthquake branches are expanded in Figure 3.7 for legibility. A similar variability is modeled to characterize variability post SCRAM after a 0.5g earthquake.

If SCRAM fails during the 0.5g earthquake, the decision tree is broken into three uncertainty clusters dealing with the reactivity coefficients selected from Section 3.1.2. The branches associated from reactivity coefficient group one is seen in Figure 3.8. The numbers in the yellow notes correspond to the simulation IDs shown in Table 5.2. While a course representation of end states are shown in the table, other information such as timing of pump failures, peak temperatures, and minimum cladding thickness can provide tradeoff information when there is insignificant deviation from course fail / no fail designations.

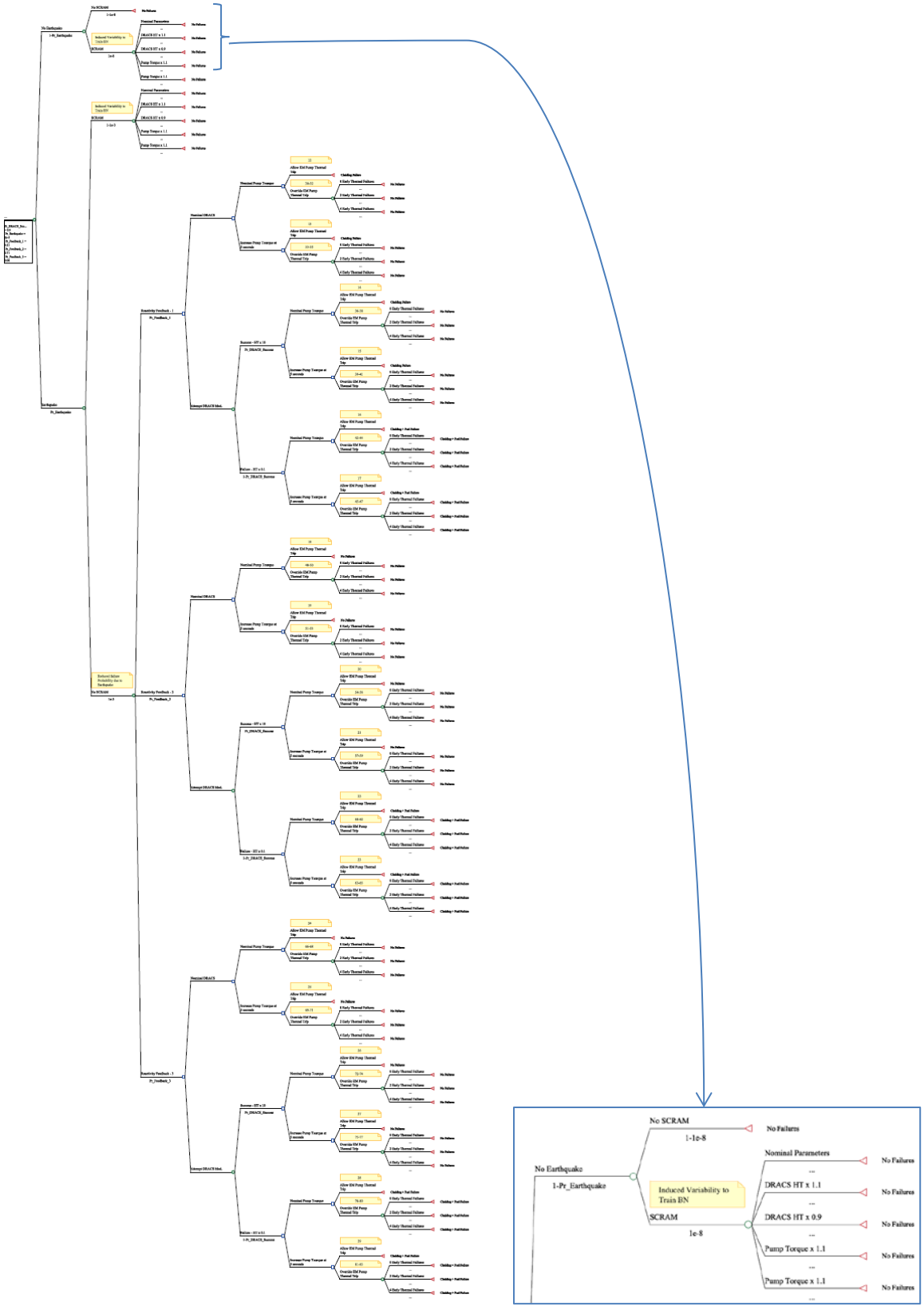

Figure 3.7 – Full SFR Decision Tree

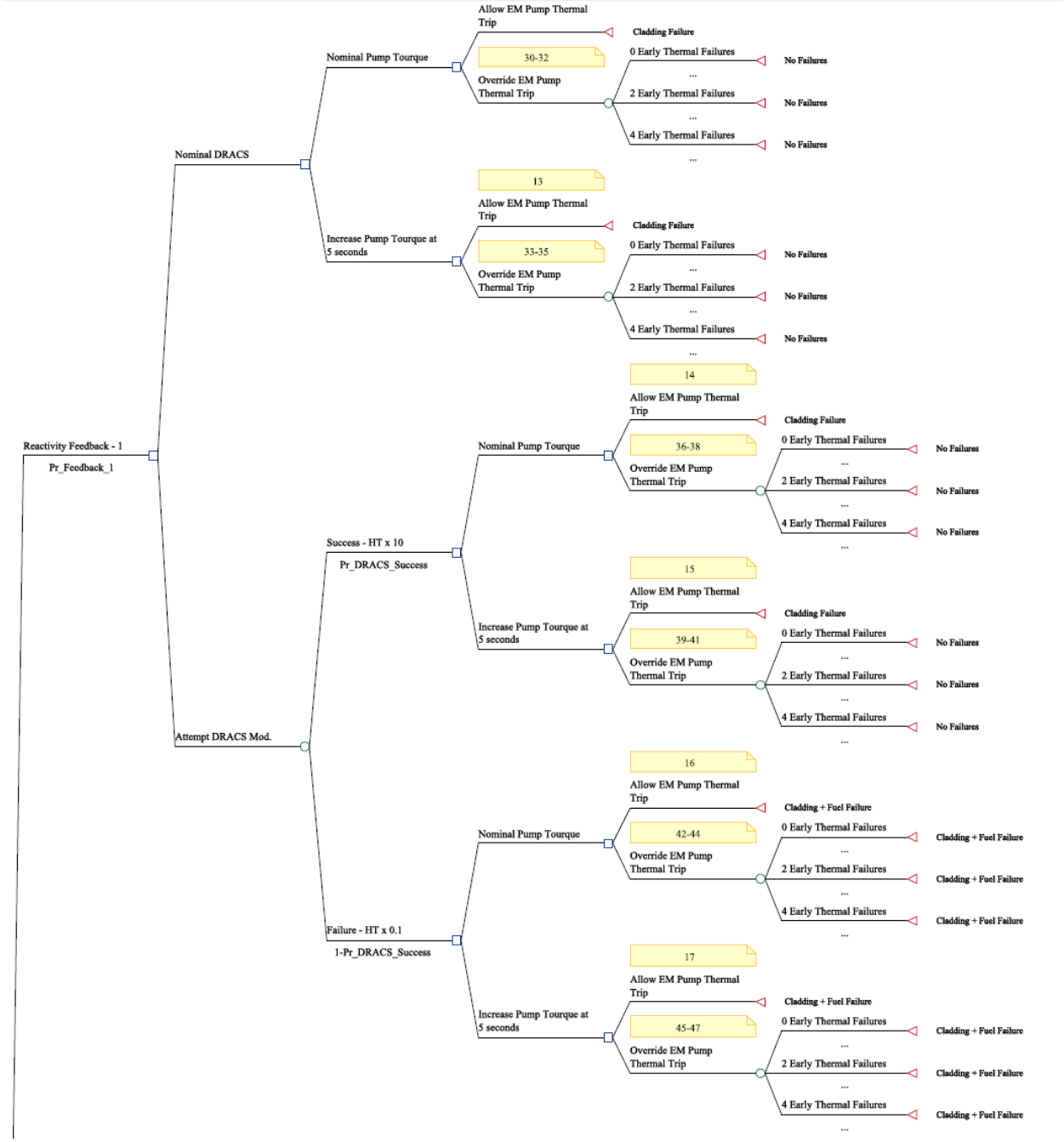

Figure 3.8 – Decision Tree Branches Associated with Reactivity Coefficient Group 1

3.3 References

[3.1] D. Grabaskas, M. Bucknor, A. Brunett, T. Sofu, A. Grelle, "Passive Safety System Reliability, Stage 1: Blackout Analysis," ANL-ARC-307, ANL, Sept. 2014.

[3.2] C. J. Mueller and D. C. Wade, "Probabilities of Inherent Shutdown of Unprotected Events in Innovative Liquid Metal Reactors," ANS Topical Meeting on Safety of Next Generation Power Reactors, Seattle WA, May 1988.

[3.3] MATLAB version 2014a, Natick, Massachusetts: The MathWorks Inc., 2010.

[3.4] E. A. Eide, S. V. Chmielewski, T. D. Swantz, "Generic Component Failure Database for Light Water and Liquid Sodium Reactors PRAs," EEG-SSRE-8875, INEL, Feb. 1990.

[3.5] Roald Wigeland, Personal Communication, January 2014.

[3.6] K. A. El-Sheikh, "Probabilistic risk assessment of the advanced liquid metal reactor, GE Nuclear Energy." GEFR-00873, 1994.

[3.7] Argonne National Laboratory, "Nuclear Engineering Division "The SAS4A/SASSYS-1 Safety Analysis Code System," ANL/NE-12/4, Argonne National Laboratory, Argonne, IL, 2011.

[3.8] G. Rodriguez, Chapter 7: Survival Models, http://data.princeton.edu/wws509/notes/c7.pdf, Sept. 2010.

4 BAYESIAN NETWORK REASONING ENGINE FOR DIAGNOSIS OF LOF ACCIDENTS

This section discusses development of a prototype model for diagnosis of Loss of Flow accidents in the generic SFR described above. In previous work [4.1], we established the theoretical framework for developing Bayesian Network-based procedures for diagnostic support for severe accidents in nuclear power plants. This section discusses the implementation of that framework to development a prototype diagnostic support model.

Advanced, simulation-based PRA methods can provide a scientific basis for supporting this diagnosis and response planning for current and future reactor designs. Recent advances in computing enable simulation-based PRA approaches to explore thousands of accident scenarios. Coupling these scenarios with plant simulations allows prediction of plant parameters and consequences associated with each accident scenario. In effect, running thousands of advanced PRA simulations allows experts to explicitly map out the relationship between known accident scenarios and observable reactor parameters. Advanced PRA offers a comprehensive understanding of accident scenarios, beyond what any single expert can provide.

This information can be harnessed to provide comprehensive, science-based support to operators facing severe accidents that fall beyond the scope of existing procedures, training, and experience. By formally encoding advanced PRA knowledge in SAMGs, we reduce the socio-technical challenges associated with responding to severe accidents, and provide an additional line of defense against events which have traditionally been related to Beyond Design Basis or residual risk.

4.1 Summary of Methodology

The methodology, as shown in Figure 4.1, takes outputs from advanced PRA and aggregates them into a Bayesian Network decision-support framework. The researcher teams develops and executes a full spectrum of DDET/SAS4A runs to cover the expected state-space of the accident. This information is used in combination with PRA information, e.g. system failure probabilities, to provide a detailed, probabilistic model of the accident sequence space. The resulting BN model is an extensive knowledge base covering a wide spectrum of possible accidents. This BN is a decision support system, which encodes the best-available knowledge from PRA to be used when needed.

In this work, the advanced PRA method uses DDETs coupled with SAS4A simulator. This coupled approach provides a process for extensive and comprehensive modeling of both the accident space and the plant response in a decision tree framework. However, due to the complexity of models used in simulation-based PRA, this in-depth understanding cannot be simulated and processed in real-time. BNs are used to synthesize and reduce this information into a framework that can be used for faster-than-real-time decision support.

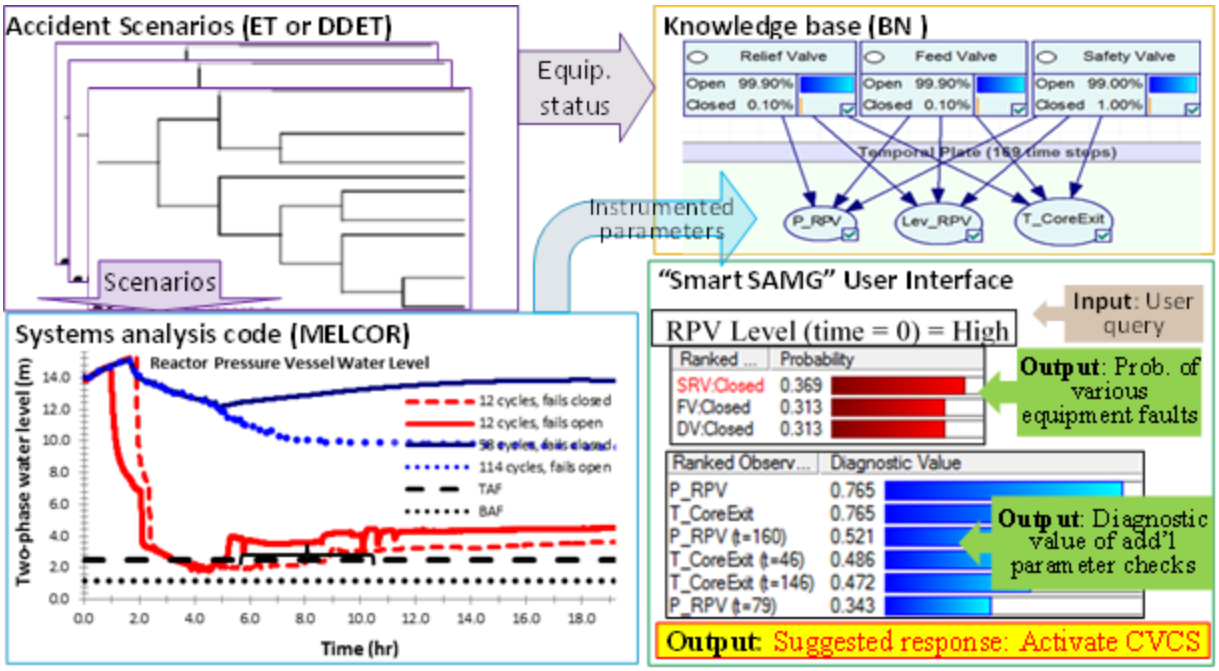

Figure 4.1 - Illustration of conceptual process to develop of risk-informed "Smart SAMG" procedures for nuclear power plant diagnostic support.

4.2 Prototype SFR model

The reactor being modeled is a generic, small modular SFR with some features adopted from the Advanced Liquid Metal Reactor (ALMR) for this work. Some key features relevant to the BN are:

- Four Electromagnetic Pumps (may fail above 500^{o}C operating temperature)
- Passive decay heat removal system uses natural circulation to transfer heat to air.
- Inherent reactivity shutdown – the reactor system exhibits strong negative reactivity feedback to increases in overall system temperature, thus the reactor can move from fission to decay heat levels without control rod insertion.

The prototype model is intended to support the diagnosis Loss of Flow (LOF) and Transient Overpower (TOP) accidents (which may or may not be concurrent) after occurrence of an earthquake.

4.2.1 Model structure & node definitions

Figure 4.2 illustrates a dynamic conceptualization of the LOF diagnosis problem. This figure contains a plate-based dynamic BN modeling the relationship between six reactor systems and components (DRACS, four EM pumps, and the scram system), one unmonitored physical state (differential pressure), five monitored plant parameters (Pressure, coolant temperature, fuel temperature, power, and reactivity),and two accident states (transient overpower and loss of flow).

The model structure shows that the four EM pumps influence the amount of differential pressure; we assume each pump has the same influence on the differential pressure. The temporal plate indicates that the time-varying reactor parameters are duplicated to 60 time steps, each representing one hour in the accident evolution. DRACS availability, scram status, and differential pressure each influence the state of all five plant parameters at each time step in the model. In this example model, the status of the DRACS, scram system, EM pumps remain constant throughout the duration of the accident (i.e., they are either failed or operational a priori, they do not fail during the accident). The scram system influences the state of the TOP node; this represents the definitional relationship wherein an unprotected TOP is defined by failure of the scram system. Similarly, the differential pressure influences the LOF state via a direct definitional relationship.

Prototype models were developed in GeNIe [4.2], which is a Windows-based development environment for graphical decision-theoretic models developed by the Univesity of Pittsburgh Decision Systems Laboratory. GeNIe implements the SMILE library of decision-theoretic method (including BNs) for the development of intelligent systems.

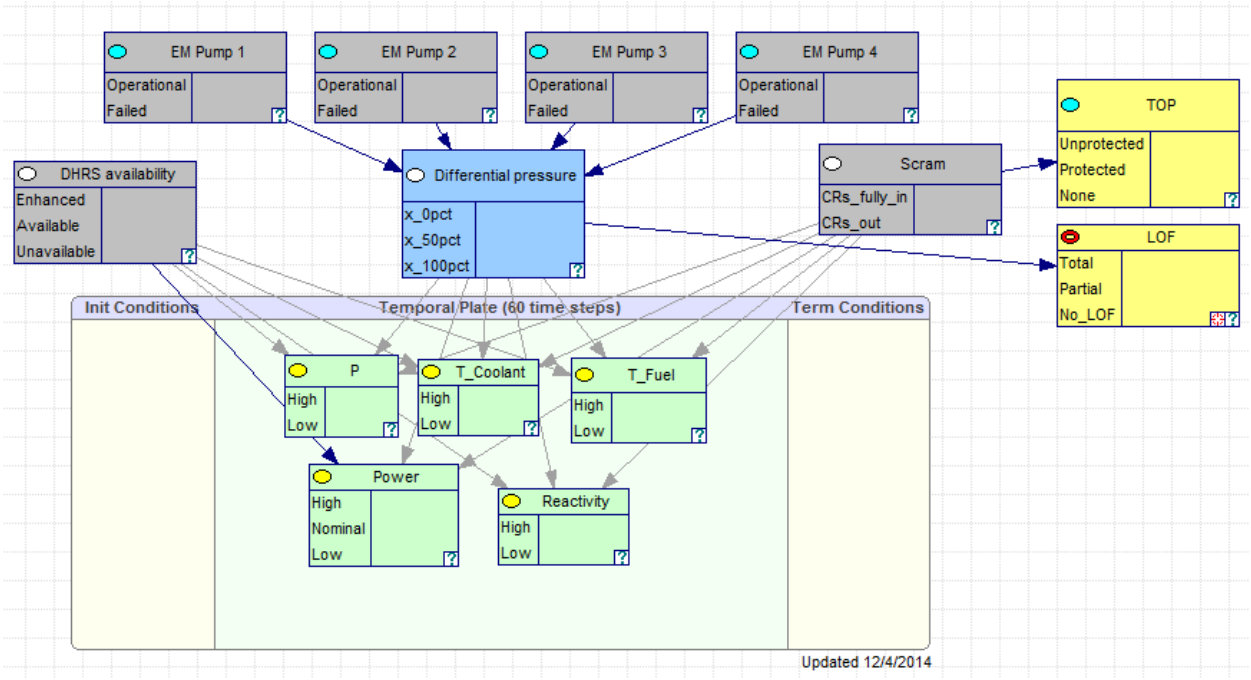

Figure 4.2 - Prototype Bayesian Network structure for diagnosis of LOF and TOP accidents in an SFR.

4.2.1.1 Accident nodes

The two accident nodes (denoted by yellow nodes in Figure 4.2) are TOP and LOF. The BN model is intended to support diagnosis of these two accidents types, which are not directly instrumented in the reactor. These two nodes are modeled as target nodes in GeNIe; this indicates that these nodes are the target of diagnosis activities. The states of these nodes are documented in Table 4.1. All degraded or failed states are assigned as target states. LOF is a deterministic node defined fully by the state of the differential pressure node. TOP is a chance node defined probabilistically based on the state of the scram system.

Table 4.1 – Definition of nodes and states for accident nodes in Figure 4.2.

Name	Meaning	States (Bold denotes target state)
TOP	Transient overpower accident. Power is increasing due to control rods being removed from the core, rod oscillation, and/or core geometry changes during a large earthquake.	**Unprotected** - No Scram (Control rods not inserted) **Protected** - Scram occurs (Controls rods are fully inserted.) None – Transient overpower accident is not occurring.
LOF	Loss of flow accident. Loss of differential pressure due to loss of one or more EM pumps. Results in loss of heat removal capacity.	**Total** – No flow(approximately 0% of required flow) **Partial** – Some flow, significantly less than required flow (approximately 50% of required flow) No_LOF – Adequate flow (approximately 100% required flow).

4.2.1.2 Systems and components

The current model contains six systems and components (denoted by grey nodes in Figure 4.2): the DRACS, four EM pumps, and Scram system. The interpretation of these nodes is discussed in detail in Section 3.1. The states of these nodes are described in Table 4.2. We assume that each of these systems is not instrumented in the reactor (i.e., the state is ascertained by monitoring the variables in Section 4.2.1.3). Each of these systems and components is defined by a Boolean node. For those that are target nodes, the target state is set as the failed or unavailable state.

Table 4.2 - Definition of nodes and states for system and component nodes in Figure 4.2.

Name	Meaning	States (Bold denotes target state)	Node type
DRACS availability	The passive decay heat removal system is available to provide cooling via natural circulation.	Enhanced – Operators successfully increase heat transfer (10x design). Available – System is available and transfers heat as designed. **Unavailable** – Minimal heat transfer (0.1x design**)**	Auxiliary
EM pump 1	Status of EM pump 1: Is it delivering flow?	Operational **Failed**	Target
EM pump 2	Status of EM pump 2: Is it delivering flow?	Operational **Failed**	Target
EM pump 3	Status of EM pump 3: Is it delivering flow?	Operational **Failed**	Target
EM pump 4	Status of EM pump 4: Is it delivering flow?	Operational **Failed**	Target
Scram	Denotes functioning of the scram system.	CRs_fully_in - Controls rods are fully inserted **CRs_out** - Control rods not inserted	Target

4.2.1.3 Monitored parameters

The current model contains five reactor parameters (denoted by green nodes in Figure 4.2). We assume that each of these parameters is instrumented in the reactor and is monitored by the control room crew. The states of these nodes are provided in Table 4.3. Definition of range discretization (binning) for the state definitions will be based on the results of the SAS4A analyses. These are observation nodes in GeNIe; the users of the model will observe values of one of more of these nodes to facilitate diagnosis of the target nodes.

Table 4.3 - Definition of nodes and states for monitored parameter nodes in Figure 4.2.

Name	Meaning	Range [nominal value]	States
P	Pressure in primary system	(1.3-0.9) [1 atm]	High Low
T_Coolant	Coolant temperature	300-900 ºC [510 ºC]	High Low
T_Fuel	Fuel temperature	300-900 ºC [580 ºC]	High Low
Power	Reactor power level	0% - 600% [100%]	High Nominal Low
Reactivity	Reactivity Feedback	See reactivity groups in Table 3.6.	**Degraded --** Mostly positive reactivity feedback Nominal - Around the expected reactivity (MLE of three coefficients) Optimistic - Mostly negative reactivity feedback

4.2.1.4 Physical states/conditions

The current model contains one physical condition, differential pressure (denoted by blue nodes in Figure 4.2). This physical condition is not instrumented or monitored; in essence it is an unobserved condition of the reactor. It is modeled as an auxiliary node in GeNIe. This node is included to ensure mode realistic capturing of the causal relationships between the monitored parameters and the possible accident sequences.

Table 4.4 Definition of nodes and states for physical condition nodes in Figure 4.2.

Name	**Meaning**	**States**
Differential Pressure	Differential pressure resulting from EM Pumps. Results in loss of heat removal capacity.	x_0%– No flow(approximately 0% of required flow) x_50% – Some flow, significantly less than required flow (approximately 50% of required flow) x_100%– Adequate flow [approximately 100% required flow].

4.2.2 Model quantification

Tables in this section document the conditional probability relationships in the BN model for each of the nodes. BN development is an ongoing process, so many of these probabilities are expected to be modified as additional analysis is conducted.

4.2.2.1 Baseline Conditional Probability Tables

The conditional probabilities for differential pressure are derived directly from the causal relationships between flow from the EM Pumps and differential pressure. High probabilities (0.95 and above) are assigned to the expected state of differential pressure based on EM Pump status To accommodate the possibility that unmodeled factors could impact the relationship between EM pumps and differential pressure, a nominal probability (ranging from 0.0001 to 0.025) was assigned to some states.

Table 4.5 - Conditional probability table for differential pressure

EMPump1	Operational								Failed							
EMPump2	Operational				Failed				Operational				Failed			
EMPump3	Operational		Failed		Operational		Failed		Operational		Failed		Operational		Failed	
EMPump4	Op.	Fail	Op.	Fail	Op.	Fail	Op.	Fail	Op.	Fail	Op.	Fail	Op.	Fail	Op.	Fail
x_0%	0	0	0	0	0	0	0	0.025	0	0	0	0.025	0	0.025	0.025	1
x_50%	0.0001	0.99	0.99	0.25	0.99	0.25	0.25	0.025	0.99	0.25	0.25	0.025	0.25	0.025	0.025	0
x_100%	0.9999	0.01	0.01	0.75	0.01	0.75	0.75	0.95	0.01	0.75	0.75	0.95	0.75	0.95	0.95	0

Table 4.6 - Conditional probability table for DHRS availability

Enhanced	0.15
Available	0.8
Unavailable	0.05

The conditional probabilities for DRACS availability were selected by an expert. Values will be updated as additional sources of information on DRACS reliability in SFRs become available.

Table 4.7 - Conditional probability table for EM Pumps

	Modeled after:	Entered in GeNIe
Operational	=1-P(failed)	=1-P(failed) =0.999999
Failed	approximately logn(mu=-12.4926, sigma=1.39975)	=1e-06

The deterministic conditional probability table for LOF is deterministic; meaning the state of LOF is completely determined by the state of differential pressure. If there is approximately 0% of the required differential pressure, a Total LOF has occurred. If there is approximately 50% of the required differential pressure, a Partial LOF has occurred. If there is approximately 100% of the required differential pressure, there is no LOF.

Table 4.8 - Conditional probability table for occurrence of LOF

Differential pre...	x_0pct	x_50pct	x_100pct
Total	◉	○	○
Partial	○	◉	○
No_LOF	○	○	◉

Table 4.9 - Conditional probability table for occurrence of scram

CRs_full_in	0.999
CRs_out	0.001

Probability of scram (during an earthquake) was assigned by expert estimation.

Table 4.10 - Conditional probability table for occurrence of TOP

Scram	CRs_fully_in	CRs_out
Unprotected	0	0.9
Protected	0.98	0
None	0.02	0.1

Probability of TOP was assigned by expert estimation.

4.2.2.2 Monitored Parameters

For the monitored reactor parameter nodes, the SAS4A data are post-processed into matrices mapping known DHRS availability, differential pressure, and scram status onto the three plant parameters at each time step. An example of this is shown in Table 4.11, in which each row represents a single SAS4A simulation, with the known configuration shown in the first three columns. The next five columns (Power_0,…, Power_4) show the power at the first five time steps from the SAS4A simulation (discretized according to the rules discussed in the previous section). The full results table contains and one column for each parameter at each time-step. Multiple simulations are run for each possible system configuration to ensure comprehensive coverage of uncertainties. The results in Section are being post-processed to fully populate these tables. Results from Table 5.2 will be further post-processed to populate the conditional probability relationships between monitored parameters and known reactor states.

4.3 Next Steps in BN Modeling

BN modeling development is ongoing, with primary focus on incorporating results from the sensitivity analysis and from the SAS4A simulations (Section 5) into the BN model. This activity includes laying foundations for the automated import of SAS4A simulation results into a BN model to streamline model quantification process for analyses of a larger spectrum of accident sequences. Additional analyses will be performed under DOE work package AT-15SN200304 to refine the range of the parameter bins based on the SAS4A results.

Table 4.11: Partial illustration of tabular representation of the aggregated results from SAS4A simulations. (Full table has one column for each parameter at each time step, and one row for each simulation run)

DHRS availability	Differential pressure	Scram	Power_0	Power_1	Power_2	Power_3	Power_4
Available	x_0%	CRs_full_in	High	Nominal	High	High	High
Available	x_0%	CRs_out	High	Nominal	Nominal	High	High
Available	x_50%	CRs_full_in	High	High	Nominal	High	Nominal
Available	x_100%	CRs_out	High	Nominal	Nominal	Nominal	Nominal
Unavailable	x_0%	CRs_full_in	High	Nominal	Nominal	Nominal	Nominal
Unavailable	x_50%	CRs_out	High	Nominal	Nominal	Nominal	Nominal
Unavailable	x_100%	CRs_full_in	High	Low	Nominal	Nominal	Nominal
Enhanced	x_100%	CRs_out	Nominal	Nominal	Nominal	Nominal	Nominal
Unavailable	x_100%	CRs_full_in	Nominal	Nominal	Nominal	Nominal	Nominal

Once full results from Section 5 have been incorporated in the BN model via the streamlined quantification process, we will use the baseline model to perform initial inference activities designed to quantify the impact that specific parameters have on the ability to differentiate between different accident conditions. After obtaining these initial results, we will prune unnecessary parameters from the model, and will subsequently begin work to extend the logic in the prototype model to accommodate failed indicator states for the monitored parameters.

4.4 References

[4.1] K. M. Groth, M. R. Denman, J. N. Cardoni, T. A. Wheeler, Proof of Principle Framework for Developing Risk-Informed Severe Accident Management Guidelines, SAND2013-8324, Sandia National Laboratories, Albuquerque NM, Sept. 2013.

[4.2] M. J. Druzdzel. SMILE: Structural modeling, inference, and learning engine and GeNIe: a development environment for graphical decision-theoretic models. In *Proceedings of American Association for Artificial Intelligence (AAAI-99)*, pages 902–903, 1999.

5 SAS4A RESULTS

SAS4A calculations are conducted to provide realistic SFR accident characteristics to the Bayesian Network. The SAS4A calculations populate an event tree for various accident scenarios, operator actions, and dynamically-determined bifurcations in accident progression such as thermal pump failure. This section presents the results of the SAS4A analyses.

The SAS4A analyses for the event tree are aimed at earthquake-induced UTOP scenarios followed by long-term reduction in heat removal, such as loss of balance of plant, degraded DRACS operation, and primary pump trip. Prior to conducting the main event tree calculations, a sensitivity analysis is conducted to help inform the branch values for the reactivity coefficients and thermal pump failure. The event tree calculations are executed to 48 hours of simulation time, while the sensitivity calculations are only executed for 1000 s. Therefore, the sensitivity analysis also facilitates a closer examination of core behavior during the early portion of the accident (i.e. during the reactivity excursion). The accident scenarios in the event tree build on short-term UTOP initiator by following it with a prolonged loss/reduction of heat removal, which is examines more plant-level phenomena that has much longer time scales.

Results of the sensitivity analyses are presented in Section 5.1. The sensitivity calculations provide some branch values for the main event tree calculations in Section 5.2.

5.1 Sensitivity Analysis of Reactivity Coefficients

The sensitivity analysis is comprised of 1000 SAS4A calculations with varying reactivity coefficients for a UTOP scenario due to a large earthquake. The analysis is separated into two sets of 500 samples: one set reflects correlated sampling between the axial and radial expansion coefficients and the other set has no correlation between the sampled values. The uncertainty distributions and sampling of the reactivity coefficients is discussed in Section 3.1.2

Uncertainties in fuel Doppler, sodium density, axial fuel expansion, and radial core expansion are considered in the sensitivity study. Feedback due to control rod expansion into the core is neglected since the effects of control rod movement are subsumed in an earthquake-induced reactivity insertion function that reflects axial rod oscillations. Multipliers are taken from the analyses in Section 3.1.2 and applied to the base reactivity coefficients in the SAS4A SFR model, and 1000 distinct SAS4A inputs are generated in an automated fashion. The accident initiator in each model is a UTOP due to a 0.5 g earthquake–all input is identical excluding the reactivity coefficients.

The UTOP sensitivity calculations are executed to 1000 s after onset of the earthquake. The coolant pumps and DRACS are assumed to be operable at the start of the accident, but balance of plant is assumed to be lost after 20 s. Each simulation also assumes that thermal pump trip occurs (via control system inputs [5.1]) once SAS4A predicts cold pool temperatures in excess of 950 K; hence the time of primary pump failure is not hardwired but determined dynamically in each realization. The plant temperatures and pump trip timings calculated by the sensitivity analysis are used to develop branch values for the event tree calculations in Section 5.2.

The reactivity insertion due to the earthquake is represented using two sinusoidal functions that have markedly different frequencies and are assumed to be out of phase; these represent radial core sloshing and axial oscillation of the control rods. Radial movement of the core involves the movement of fuel assemblies relative to one another–this causes significant reactivity fluctuations since the fast spectrum is quite sensitive to variations in neutron leakage and the pitch between fuel assemblies. The axial component largely reflects the control rods oscillating in the core, but could also represent the different axial movement of fuel assemblies. The frequency of the axial reactivity function (10 Hz) is much higher than that of the horizontal function (0.75 Hz). These frequencies are adopted from PRA work for the Advanced Liquid Metal Reactor (ALMR). The maximum amplitudes of the sinusoidal functions are also adopted from the ALMR PRA (namely Table 4-7 in Reference [5.2]). Maximum reactivity amplitudes are listed in Table 5.1 for three earthquake sizes. Table 5.1 also shows the frequencies associated with each earthquake magnitude.

Table 5.1. Earthquake reactivity quantities.

Size	Frequency (yr^{-1})	Axial ($)	Radial ($)
0.3	$1x10^{-4}$	0.163	0.228
0.5	$2x10^{-5}$	0.278	0.380
1.0	$6x10^{-7}$	0.548	0.418

Figure 5.1 shows the reactivity insertion functions associated with the 0.5 g earthquake. The peak amplitudes from Table 5.1 are assumed to occur near 8 s, and simple linear multipliers are used to dampen the sinusoidal amplitudes before and after this time. The reactivity insertion due to the earthquake is nearly zero after 50 s. Figure 5.2 depicts the detail of the reactivity insertion from 0 to 10 s, and it better illustrates the very high frequency of the axial reactivity oscillations.

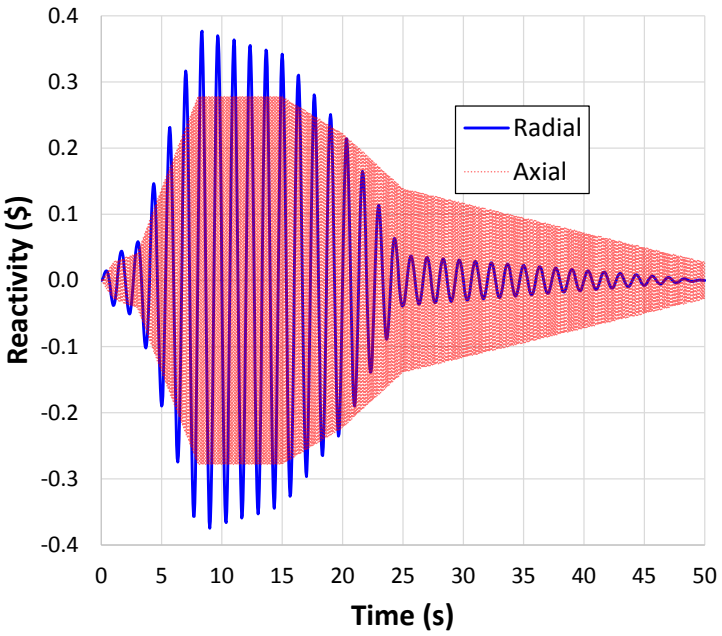

Figure 5.1. Reactivity insertion functions for 0.5 g earthquake.

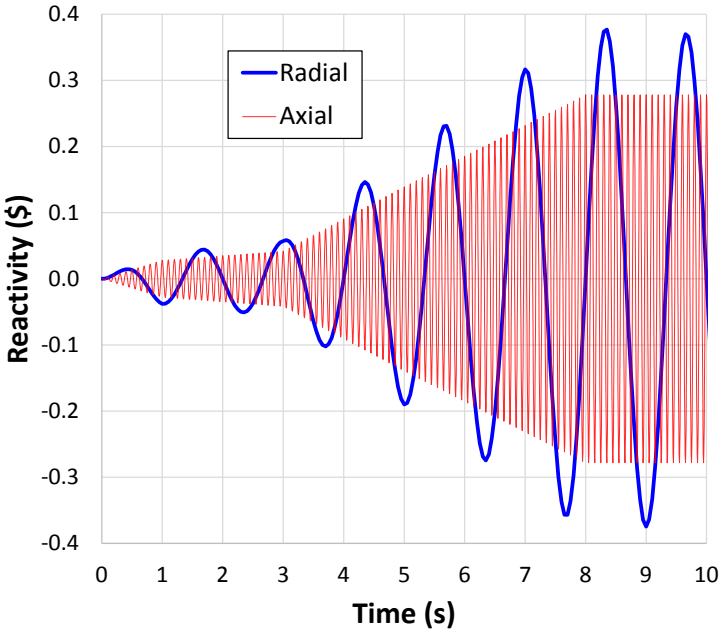

Figure 5.2. Detail of reactivity functions from 0 to 10 seconds.

Results for the 500 correlated trials are presented in Sections 5.1.1-5.1.4. The uncorrelated results are qualitatively very similar, and are therefore not discussed in this report. The uncorrelated calculations are mainly used to assess the effects of correlated sampling between the axial and radial expansion coefficients, which were determined to not induce any first-order differences in the SAS4A calculations.

The 500 SAS4A calculations are executed for 1000 s of simulation time. Seven cases did not reach this termination time due to the prediction of major coolant boiling, fuel/cladding damage, and material relocation. Thus, these 'failed' calculations are terminated early (around 20 s) and are neglected in the majority of the plots in the following sections.

5.1.1 Reactivity, Power, and Thermal-hydraulic Reponses

Total reactivities calculated by SAS4A are depicted in Figure 5.3 , which includes the sinusoidal insertions and all feedback. The sinusoidal insertions acts in conjunction with positive feedback due to increased coolant temperature (i.e. reduced sodium density) and causes overall reactivity to be mostly positive for the first 10 s of the accident, after which the other feedback mechanisms (mostly radial and axial expansion) reduce overall reactivities below zero after 25 s. Overall reactivities decrease monotonically after 100 seconds and all trials reach a quasi-equilibrium value of about -0.2$ as simulation time approaches 1000 s.

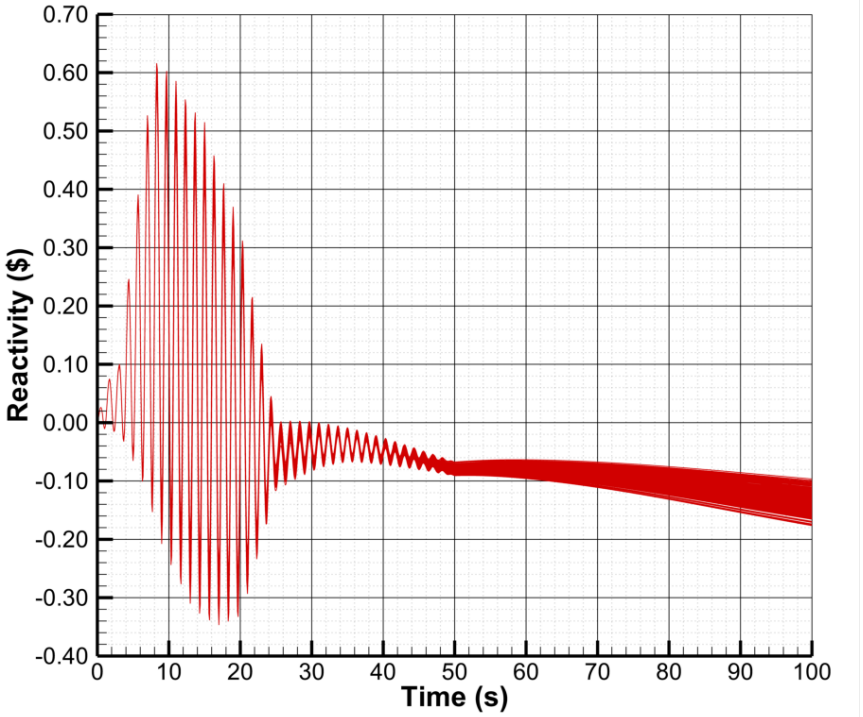

Figure 5.3. Total reactivity including feedback and external reactivity.

The associated power levels are shown by Figure 5.4. Despite the negative reactivity oscillations, relative power levels exceed 1.0 until about 60-80 s. Reactivity oscillations about zero reactivity tend to drive an overall increase in power level (rather than oscillate about 1.0) for the following reasons:

- The magnitude of the prompt jump in power for a rapid and positive reactivity insertion is greater than the prompt drop for a negative reactivity insertion of equal magnitude. This effect is explainable by the prompt jump approximation, i.e. $P_2/P_1 \approx 1/(1-\rho)$, where inserted reactivity (ρ) is in dollars and the reactor is initially critical.
- Delayed neutron power can increase at a faster rate than it can decrease for the same magnitude of reactivity insertion; this is an intrinsic characteristic of fission reactor kinetics with typical kinetic parameters for SFRs (and LWRs for that matter). Reactor period is shorter for positive reactivity insertions and is inversely proportional to the reactivity magnitude. In contrast, reactor period is longer for negative insertions, and the period is again inversely proportional to the reactivity magnitude but limited by the longest lived delayed neutron precursors–hence the rate of power decrease is also limited by the longest lived precursors for negative insertions. Figure 5 shows a SAS4A calculation of prompt reactivity insertion of ±0.2$, and it confirms the prompt jump and reactor period differences for positive and negative insertions.

These factors drive an overall power escalation for the first 20 s of the accident. They act in conjunction with the fact that the radial reactivity insertion due to core sloshing is initially positive, the axial insertion has a high frequency (which exacerbates the power “ratcheting” [5.2]), and total reactivity is more positive for the first 10 s. Figure 5.4 shows that power

decreases monotonically from 50 to 100 s, after which power level stays below 1.0 for all trials since total reactivity remains below zero for the remainder of the simulation time.

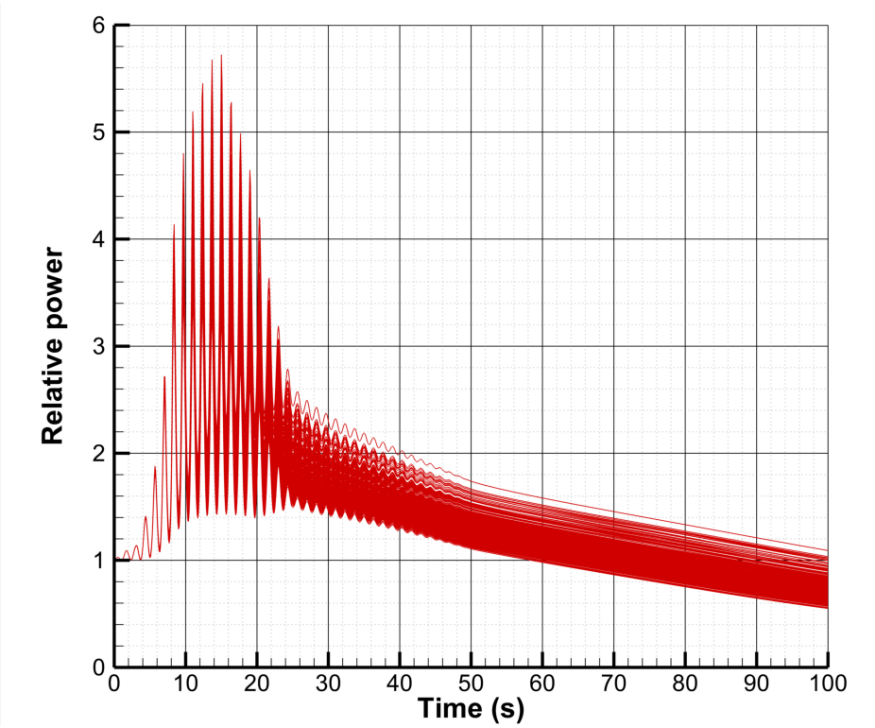

Figure 5.4. Power level for 0-100 s.

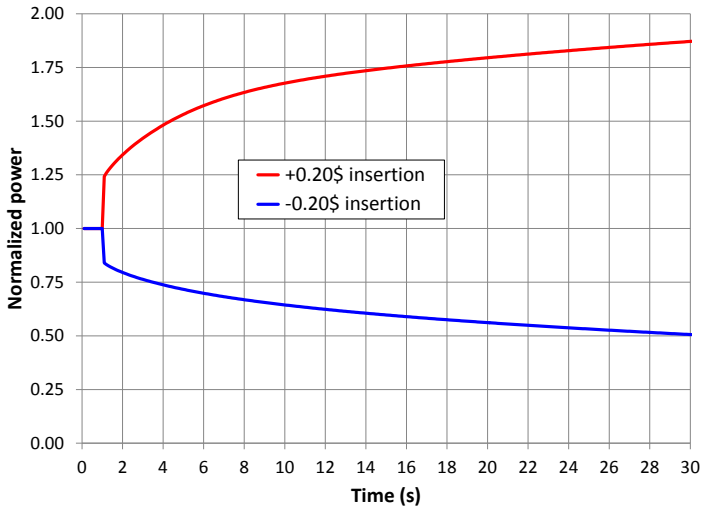

Figure 5.5. Power response to sudden reactivity insertion calculated by SAS4A.

Figure 5.6 shows peaks fuel temperatures, and Figure 5.7 depicts maximum coolant temperature in the core channels. Rapid temperature escalation due to the earthquake reactivity, positive sodium feedback, and power ratcheting is apparent near the start of the accident. Peak fuel temperatures in this period range from 1130 K to 1400 K, and peak coolant temperatures range

from 1010 K to 1230 K. None of the trials depicted on these figures exhibit bulk coolant boiling and core damage. However, seven trials did reach such a state and were terminated early due to significant fuel relocation; these trials terminated at 10 to 20 s after accident initiation and they all had high multipliers sampled on the coolant feedback coefficient, and low multipliers sampled for the negative feedback mechanisms (expansion and Doppler). The cases with large core damage are neglected in the figures in this section.

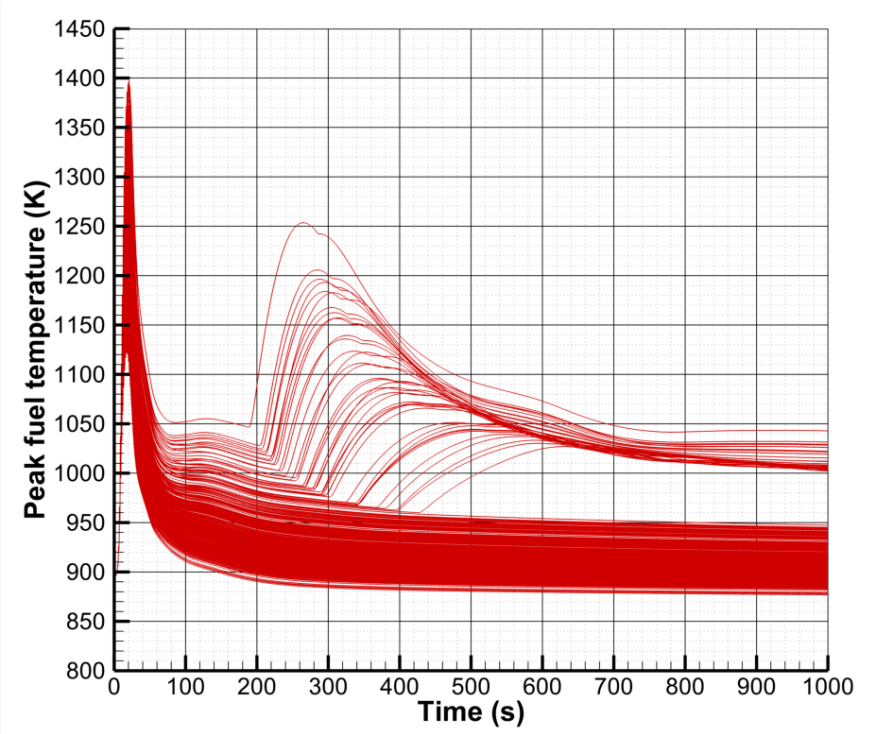

Figure 5.6. Maximum fuel temperature.

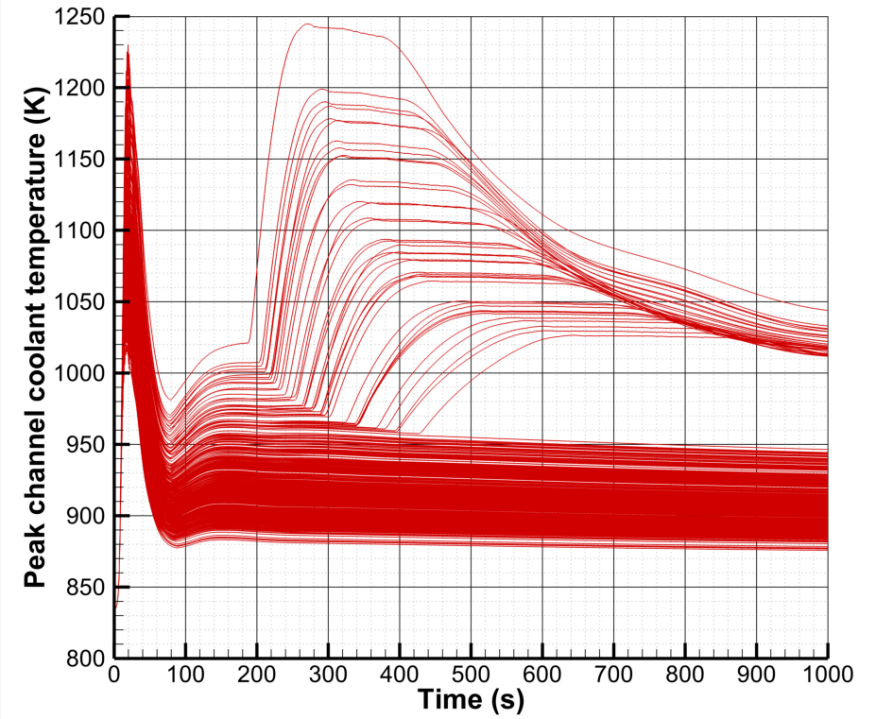

Figure 5.7. Maximum coolant temperature in core channels.

About 10% of the trials exhibit excessive cold pool temperature to trigger the assumed thermal trip of the primary pumps at 950 K; these pump trips are predicted to occur between 190 to 420 s after onset of the earthquake. All such trials have high sampled values (> 1.0) for sodium density feedback and most have low sampled values for axial and radial feedback, which leads to sufficiently higher peak powers and plant temperatures to trip the primary pumps. Hence, the second rise in maximum fuel and sodium temperatures observed for some trials in Figure 5.6 and Figure 5.7 is driven by a loss of flow, not by a second reactivity excursion. Overall reactivity remains below zero, and relative power remains below 1.0, after 100 seconds.

Power to flow ratio is an important quantity for unprotected SFR accidents. Figure 5.8 depicts power to flow ratio normalized to the nominal ratio for the whole core according to Eq. 6:

$$Power\ to\ Flow\ Ratio = \frac{P}{F} = \frac{250\text{x}10^6\ \text{W}}{1270.9\ \text{kg/s}} = 196711.8\ \frac{\text{W}}{\text{kg/s}} \tag{6}$$

It shows that the initial reactivity and power excursion due to the earthquake drives a large mismatch in power and flow–channel flow is essentially constant in each trial for the first 100 s. The loss of flow due to thermal pump trip is evident in Figure 5.8 and Figure 5.9, which shows the flow rate for the inner core (channel 1). The pump trips drive a second mismatch in power to flow ratio, thereby causing a second rise in fuel and coolant temperatures that can have further repercussions such as increased cladding damage.

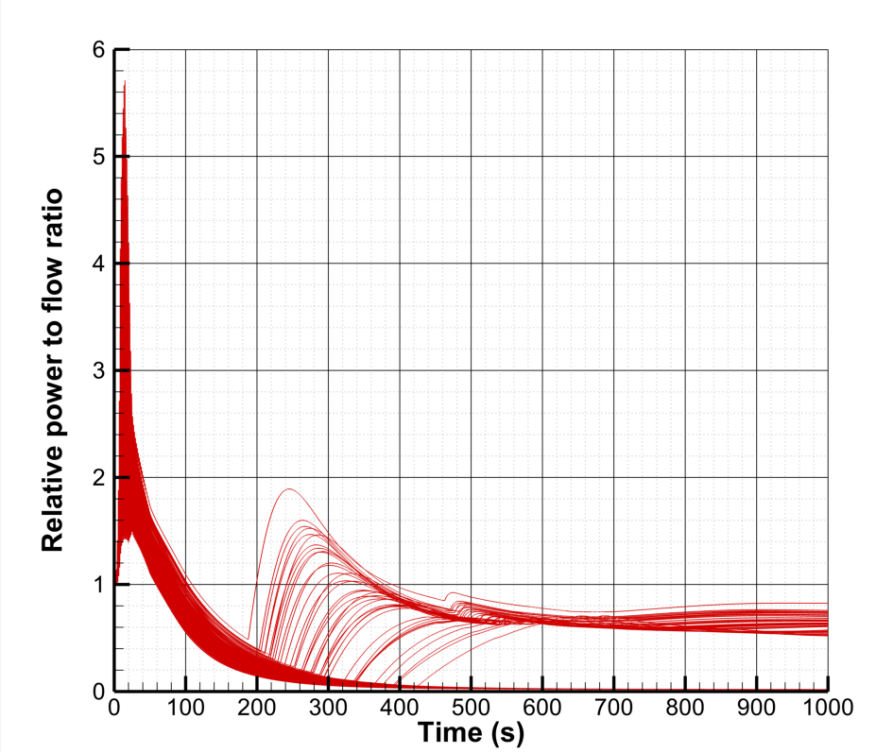

Figure 5.8. Normalized power to flow ratio.

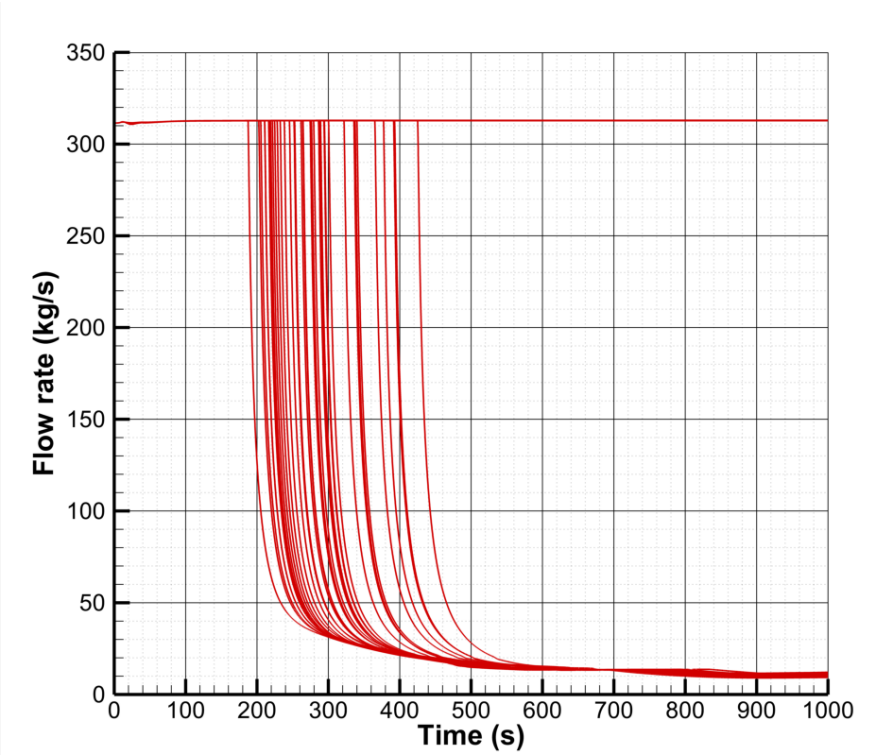

Figure 5.9. Flow rate in channel 1 (inner core channel).

5.1.2 Reactivity Feedback

The sensitivity calculations consider reactivity feedback due to coolant density, radial core expansion, axial fuel expansion, and Fuel Doppler effects. The magnitudes of these feedback mechanisms are shown in Figure 5.10, Figure 5.11, Figure 5.12, and Figure 5.13, respectively. Most of the trials (493/500) did not lead to significant boiling and core damage, and hence the fuel relocation feedback is not considered here.

The temperature coefficient of the coolant is positive in the SFR SAS4A model, which is a common characteristic of SFRs. The positive temperature coefficient reflects the fact that sodium in the core down-scatters a portion of the flux spectrum into energy regions of high resonance capture in fuel and core structures. Coolant temperatures can increase considerably for power and flow accidents, as shown in Figure 5.7, thereby decreasing the density of the sodium in the core. A decrease in coolant density reduces the macroscopic cross section of the sodium and hardens the neutron spectrum, thus increasing gross ratio of fission to capture reaction rates. The peripheral core regions can exhibit negative feedback upon heatup due to increased fast neutron leakage, but the gross reactivity feedback of the core coolant is largely positive due to neutron spectrum hardening in the inner core.

Figure 5.10 shows the positive reactivity feedback due to increased coolant temperatures in the sensitivity calculations. The spread in reactivity principally reflects the multipliers applied to the base reactivity coefficient in the SFR model, in addition to subsequent differences in thermal-hydraulic accident progression. The initial (from 0 to 30 s) positive reactivity feedback from coolant expansion is due to the earthquake reactivity insertion and the early power increase and heatup of the core. A temporary decrease in positive coolant feedback exists afterwards due to decreasing fuel and coolant temperatures; the inflection in core temperatures around 30-90 s (Figure 5.6 and Figure 5.7) is the result of total reactivity dropping and remaining below zero for the first time, which is due to feedback and termination of the earthquake insertion (Figure 5.1), in conjunction with the DRACS and primary pumps gradually removing energy from the primary system. The pump trip events after 200 s are visible and result in a second rise in coolant feedback, but this positive reactivity is compensated by the other feedback mechanisms and overall reactivity is below zero for the remainder of the simulation.

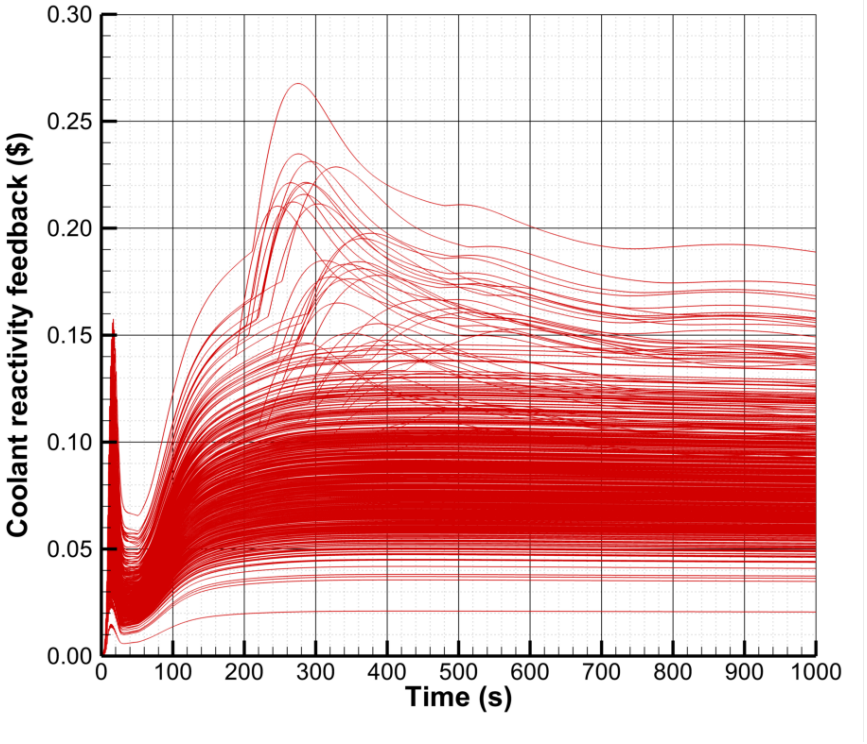

Figure 5.10. Coolant density feedback.

Radial core expansion and axial expansion of the fuel are important negative feedback mechanisms: The relatively small core and fast neutron spectrum make the system reactivity especially sensitive to changes in neutron leakage due to thermal expansion of the fuel and structures in/near the core. The magnitudes of radial and axial expansion for the sensitively study are depicted in Figure 5.11 and Figure 5.12, respectively. Both of these mechanisms insert negative reactivity into the core for much of the accident duration and work to compensate the positive coolant feedback. Thus reactivities due to axial and radial expansion are roughly an inverse reflection of the coolant reactivity; increasing core temperatures makes the expansion feedbacks more negative, while decreasing core temperatures reduces their magnitudes. The pump trips cause a second rapid rise in coolant and core temperatures, which drives higher magnitudes of negative expansion feedback.

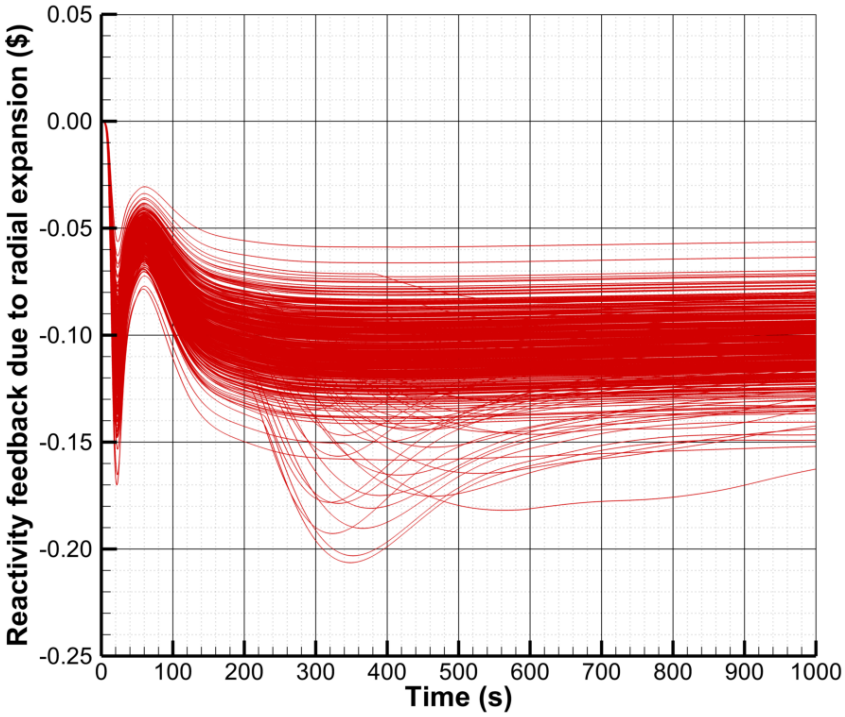

Figure 5.11. Radial core expansion feedback.

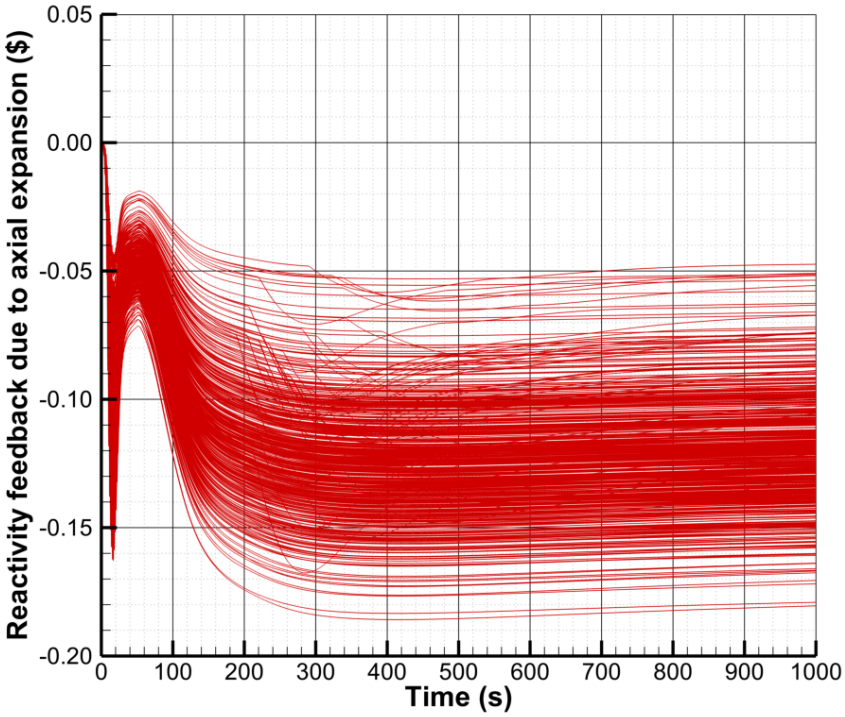

Figure 5.12. Axial fuel expansion feedback.

The feedback due to Doppler broadening of neutron capture resonances in the fuel is generally small (compared to LWRs) and negative in SFRs. Negative Doppler feedback in the SFR model for this work is significant but of lesser magnitude than radial and axial expansion. Nonetheless, fuel Doppler feedback plays an important role in rapidly counteracting increased fuel temperatures for unprotected accidents with reactivity excursions. This is evident by comparing Figure 5.13 to maximum fuel temperatures (Figure 5.6) near the start of the accident (0-30 s); the initial large increase in fuel temperatures results in a rapid and significant negative feedback from Doppler broadening (-0.10$ to -0.15$). Negative Doppler feedback is nearly instantaneous compared to the delayed coolant and radial expansion mechanisms, which depend on heat transfer processes that lag the fuel temperature. Axial fuel expansion is also a relatively fast feedback mechanism for metal-fueled SFRs [5.3].

After the earthquake reactivity insertion is over, the Fuel Doppler feedback plays a secondary role in controlling the reactor compared to the expansion feedback mechanisms: The magnitude of Doppler feedback is generally half the magnitude of the axial and radial expansion feedbacks. However, Figure 5.13 shows some outliers with rather large (≤-0.15$) Doppler feedback for later simulation times; these are the result of a few trials that have large multiplier samples applied to the Doppler coefficient. The majority of the trials exhibit Doppler feedback near -0.05$ for later simulation times (i.e. after 100 s). In comparison, Figure 5.11 and Figure 5.12 show that radial and axial expansion feedbacks after 100 s are predominately around -0.10$ and -0.13$, respectively.

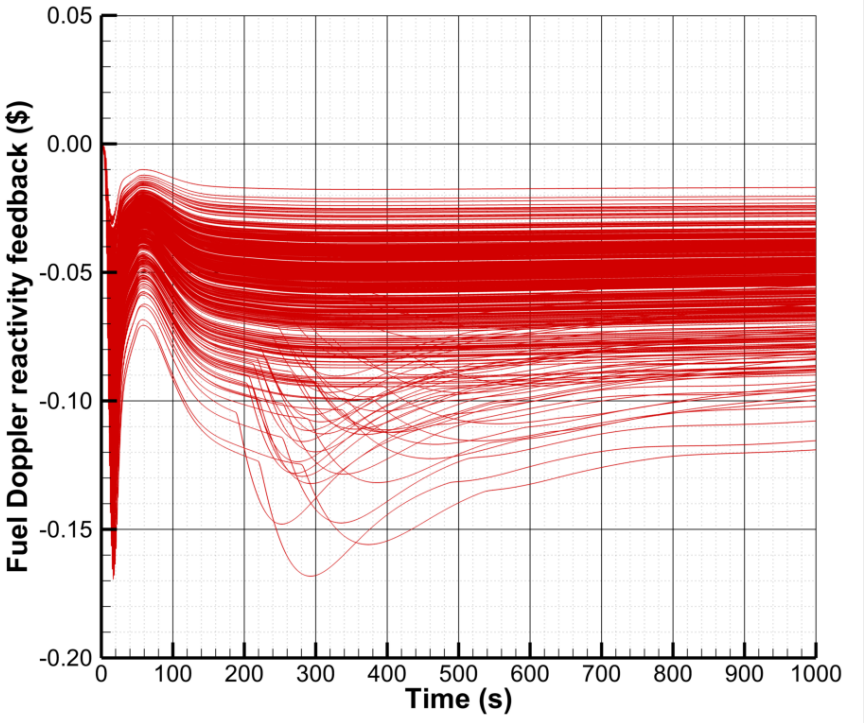

Figure 5.13. Fuel Doppler feedback.

5.1.3 Eutectics and Cladding Thickness

The increased core temperatures drive fuel-cladding eutectic reactions that reduces the overall thickness of the cladding. Cladding wastage for the sensitivity study is depicted in Figure 5.14. The peak power to flow channel (channel 5) exhibits the most cladding degradation at the core exit; the metal fuel generally causes axial core temperatures to peak near the core exit. Two distinct periods of increased eutectic penetration rate are apparent: The initial reactivity and power excursion from 0 to 30 s and after thermal pump trip, which occurs in about 10% of the trials after 190 s. All cases with thermal pump trip exhibit the second, later period of cladding wastage, and these cases are highlighted in blue in Figure 5.14. Another important feature evident in Figure 5.14 is a flat-lining of cladding thickness for several of the trials that undergo pump trip. This feature signifies local cladding failure due to hoop stress. Subsequently, cladding failures may occur in the lower axial nodes and/or in the other channels. 11 cases have early cladding failure at the top node of channel five due to the power excursion, and thus these cases appear as the blue curves (since they also have pump trips later) in Figure 5.14 that flat-line near 20 s at cladding thickness near 0.49 mm. Further cladding wastage and failures continue in other axial nodes and channels in these cases.

Figure 5.15 depicts the same plot but has cases with cladding failure highlighted in blue. The cladding failures are mostly limited to the top 5-6 axial nodes of the peak and inner core channel. However, some trials exhibit cladding failure of the upper nodes in all of the fueled channels in the model. There are 21 cases with cladding failure out of the 493 total successful cases. Naturally, the 7 cases that have significant coolant boiling and fuel damage also have widespread cladding failures.

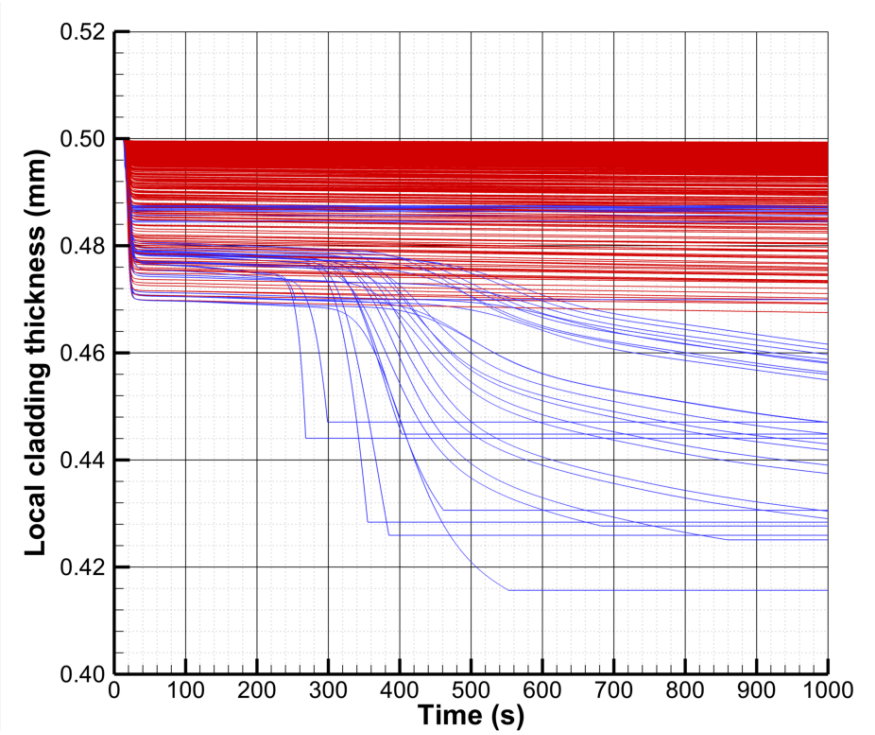

Figure 5.14. Cladding thickness in channel 5, top axial node.

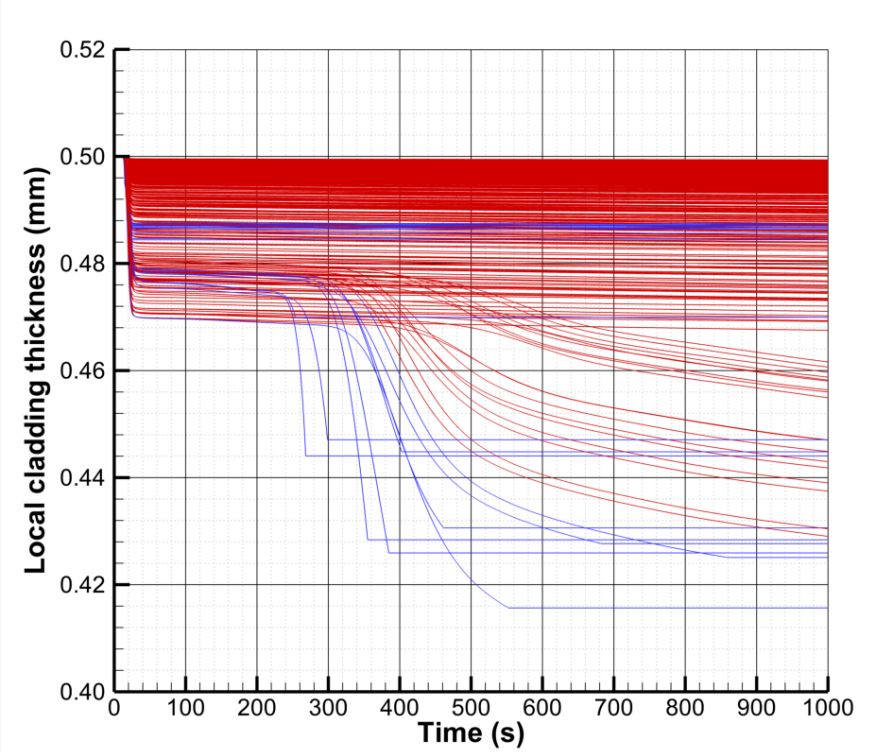

Figure 5.15. Cladding thickness in channel 5, top axial node.

Figure 5.16 isolates the cases with pump trip; blue curves denote cladding failure.

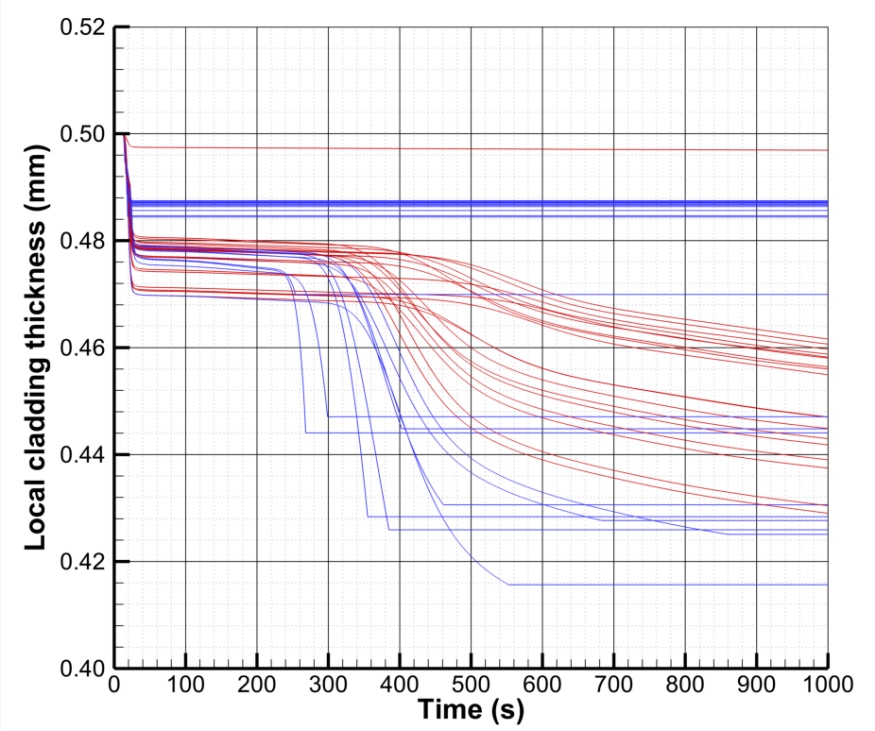

Figure 5.16. Cladding thickness in channel 5, top axial node; cases with pump trip.

5.1.4 Scatter Plots

Examination of model inputs and key outputs reveals fairly monotonic and intuitive behavior. As expected, cases with low sampled multipliers on the reactivity coefficients for axial/radial expansion and Doppler (i.e. the negative feedback mechanisms), in conjunction with high sampled multipliers for the sodium reactivity coefficient (the positive feedback mechanism), yield exacerbated reactivity/power excursions and degraded plant conditions. Figure 5.17 shows a 3D scatter plot of the 500 (including the 7 cases that lead to fuel failure) sampled inputs for the multipliers on the axial fuel expansion, radial core expansion, and sodium feedback coefficients. Doppler feedback is also important but of lower overall magnitude, and hence its influence is not explicitly shown in Figure 5.17. Each point in Figure 5.17 has a color contour applied that reflects the maximum fuel temperature predicted by SAS4A in each case. The 7 cases that experience fuel failure are evident as the dark orange and red dots, which all have high sampled values for the positive sodium coefficient; these are the only cases that exhibit fuel temperatures in excess of 1400 K, which result from significant coolant boiling and the subsequent reactivity/power excursion.

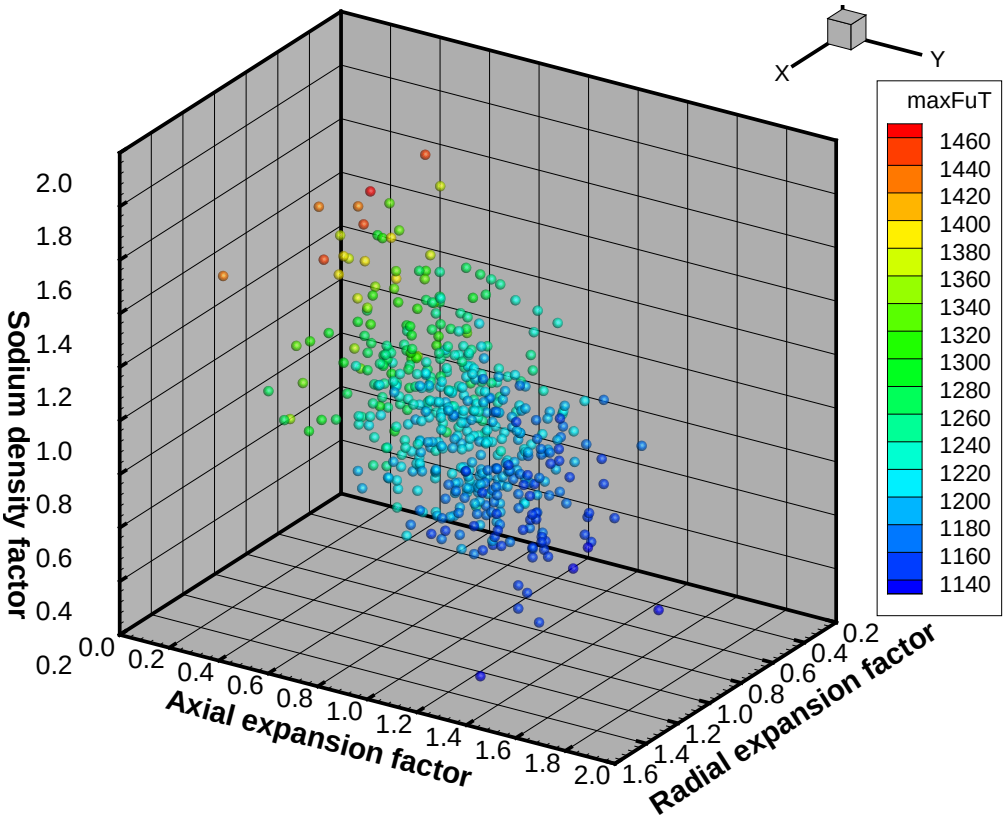

Figure 5.17. Scatter plot of key inputs with color contour of maximum fuel temperature.

The spatial scatter of the points in Figure 5.17 is random and normally distributed since the three axes are just the input values that are sampled by Monte Carlo. The color contour demonstrates that SAS4A is predicting a rather monotonic relationship between the reactivity coefficient multipliers and maximum fuel temperature. Cases with high multipliers on the negative feedback

mechanisms lead to lower maximum fuel temperatures and vice-versa for the positive sodium feedback. Slight non-monotonic behavior is readily explainable by the sampled multipliers for the Doppler coefficient.

Figure 5.18 depicts a similar 3D scatter plot, except the color contour now reflects the final (at 1000 s) state of the cladding, as predicted by SAS4A. Blue dots signify coolant boiling, cladding failure, and fuel failure/relocation. Green dots indicate cases with cladding failure, some of which have small amounts of sodium boiling. The red dots are cases with no major cladding failure, but some of these cases do exhibit significant cladding wastage through eutectic reactions. Again, it is clear that high sampled values (over approximately1.5) for the sodium coefficient multiplier produce more cladding failures, especially when the thermal expansion multipliers are less than 1.0. The influence of the Doppler multiplier is slightly less significant but it does contribute to a few outliers, such as a few cases with high sodium coefficient that avoid cladding failure. High Doppler multipliers assist in lowering reactivity and preventing excessive temperatures. There are also a few cases that have rather low sodium coefficients (< 1.2) but still undergo cladding failures; these are the result of low multipliers for the negative feedback mechanisms including Doppler feedback.

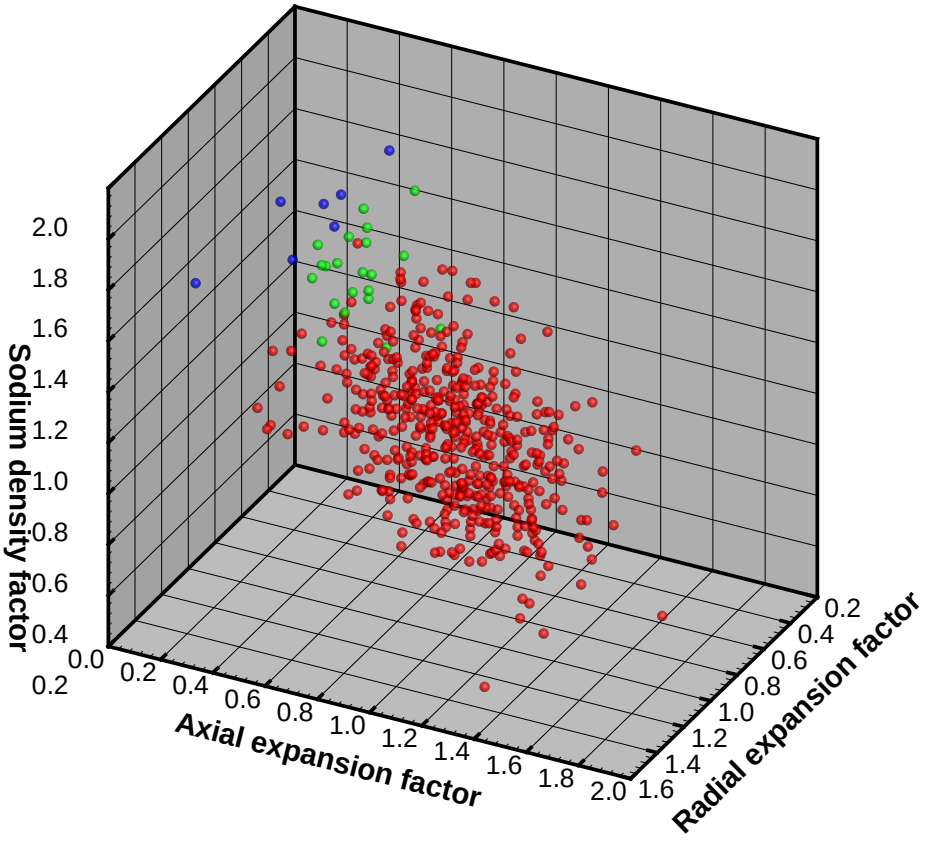

Figure 5.18. Scatter plot of key inputs with color contour of final cladding status.

5.2 SAS4A Results for Main Event Tree

The main event tree is comprised of 83 distinct SAS4A simulations with various boundary conditions, some of which are determined dynamically by SAS4A such as thermal pump failure. The base accident scenario is the same UTOP driven by the 0.5 g earthquake that is described in Section 5.1. The event tree also includes 'nominal' scenarios with no earthquake and reactivity excursion. These nominal scenarios also assume successful shutdown, loss of balance of plant, variable DRACS operation, and variable pump throttling by the operators. Another variation of a nominal scenario is simulated that has no earthquake and no scram, but a loss of balance of plant in combination with normal DRACS and pump operation. Such scenarios are investigated in order to provide baselines for comparison between nominal and severe/perturbed branches in the Bayesian models.

The event tree simulation includes branch criteria that are informed by the sensitivity analysis in Section 5.1. Three sets of multipliers on the reactivity coefficients are derived from the sensitivity results (see Section 3.1.2.2)–these reactivity coefficients are varied in unison for the event tree. The branch parameter for thermal failure of the primary pumps is also informed by the sensitivity analysis. Thermal pump trip is assumed in some branches of the event tree calculations if SAS4A predicts cold pool temperature exceeding 878.5 K. Pump trip is also assumed as an operator action in some branches once cold pool temperature reaches 798 K. Further discussion on the branch parameters for the event tree is given in Section 3.1.

The results for the event tree have time plotted on a log scale to highlight the broad time frames of the accident on a single figure: The reactivity excursion occurs between 1 s and 50 s, pump trip effects occur between 80 s and 1000 s, and long-term cooling (or lack thereof) by the DRACS is important between 1000 s to the end of the simulation (48 hours or 1.728×10^5 s).

5.2.1 Reactivity, Power, and Thermal-hydraulic Reponses

The total reactivity and power responses for all branches in the vent tree is shown by Figure 5.19 and Figure 5.20, respectively. These figures depict branches that undergo the earthquake transient and branches that assume successful scram. A single scenario is also depicted that assumes no reactivity excursion and no scram in combination with a loss of balance of plant and nominal operation of the DRACS and primary pumps. This branch and the branches with scram provide baselines for comparative purposes in the BN model.

The blue curves in Figure 5.19 indicate branches that lead to widespread coolant boiling and fuel damage. These branches are not easily discernable on the power figure; hence Figure 5.20 does not depict the blue curves. The branches that lead to major fuel failures all have highly degraded DRACS performance: A 0.1 multiplier[3] is applied to the tube-to-air heat transfer coefficient for the ADHX; this is discussed more in the subsequent figures and sections.

[3] Preliminary calculations for the event tree used a 0.5 multiplier for the heat transfer coefficient, which did not lead to significant boiling and fuel failure. Hence, the final event tree calculations use a 0.1 multiplier to 'steer' some of the calculations to have poor end states (i.e. coolant boiling). This is done purposefully so that the BN analyses may clearly assess the impacts and potential risks of operation actions for severe accidents.

Figure 5.19 and Figure 5.20 show that the cases with nominal and enhanced (x10) DRACS lead to the reactor returning near critical after 10^4 s. The branch with no earthquake and no scram also exhibits this trend. Oscillations about zero reactivity drive some late-term and minor peaks in power. These reactivity oscillations are the product of long-term cooling by the DRACS; as plant temperatures approach their original steady-state values, the thermal feedback mechanisms result in a slight overshoot past zero reactivity, followed by small oscillations until the reactor settles at zero reactivity.

The reactivity insertions due to the earthquake are readily apparent in Figure 5.19 and Figure 5.20. As discussed in Section 5.1.1, the combined influences of the large reactivity fluctuations, fundamental nuclear kinetics, and early feedback cause reactivity to be mostly positive for the first 10-20 s of the accident, while power level climbs above 1.0 until about 70-80 s. As core and coolant temperatures increase considerably, negative feedback (and the dampening insertion, see Figure 5.1) quickly reduces the total reactivity below zero after 25-30 s. This terminates the initial power excursion, and all branches have power less than 1.0 after 80 s. Although power levels are less than 1.0 after this time, plant temperatures are still increasing due to the loss of balance of plant; DRACS is only sized to remove decay heat (6-7% of power). Therefore, cold pool temperatures reach 798 K around 80 s, at which some branches assume the operators trip the primary pump to preclude thermal failure. For branches that do not assume operator action, thermal failure temperatures (878.5 K) are reached after 180 s. The pump trips manifest themselves on the reactivity figure as sudden decreases in reactivity, which is due to negative feedback following the sudden rise in core temperatures. The reactivity effects of the pump trips do not really influence power since total reactivity is already less than zero and power level is already dropping after 80 s. The blue curves in Figure 5.19 that reach fuel damage experience strong negative feedback due to the excessive plant temperatures. The sudden drop to zero reactivity for these branches merely reflects early termination of the calculations before the 48 h simulation time.

Maximum fuel temperatures for the event tree simulation are depicted in Figure 5.21. The corresponding maximum coolant temperatures are shown by Figure 5.22. The blue curves denote branches that lead to major fuel failures, which are all branches with degraded DRACS operation. The key stages of the severe accident are apparent in these figures:

1. Earthquake reactivity insertion from 1 s to 50 s;
2. Pump trips between 80 s and 1000 s;
3. Long term cooling by DRACS to 48 h.

These severe accident features are juxtaposed with the branches that have successful shutdown, and the branch with no earthquake and no scram. It is interesting and somewhat counterintuitive to note that the branch with no earthquake/scram still reaches manual pump trip (at 798 K) around the same time (approximately150 s) as many other branches that have the earthquake power excursion.

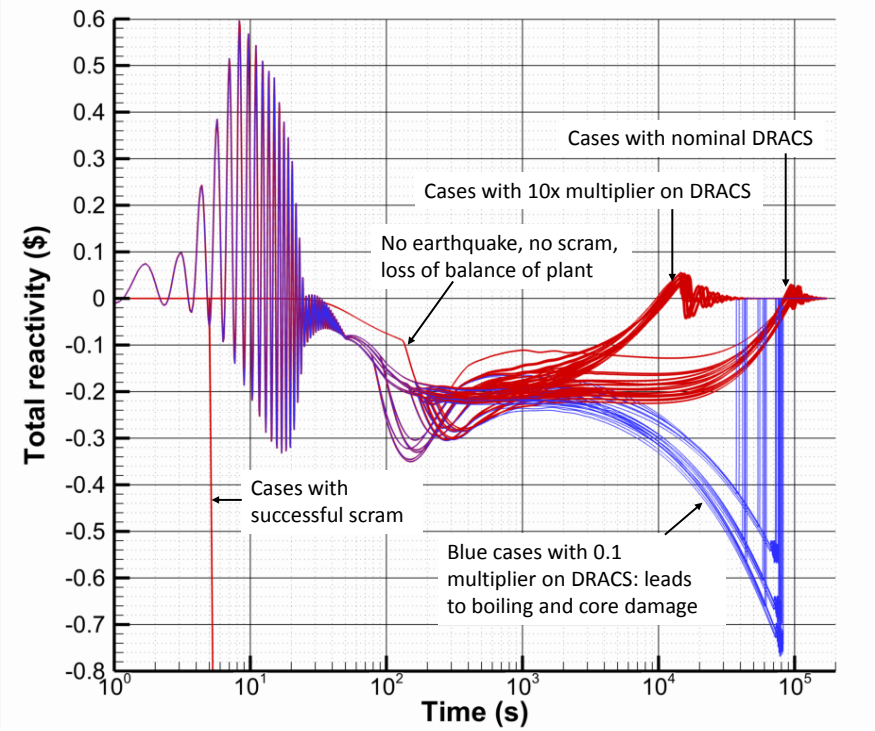

Figure 5.19. Total reactivity for event tree simulation.

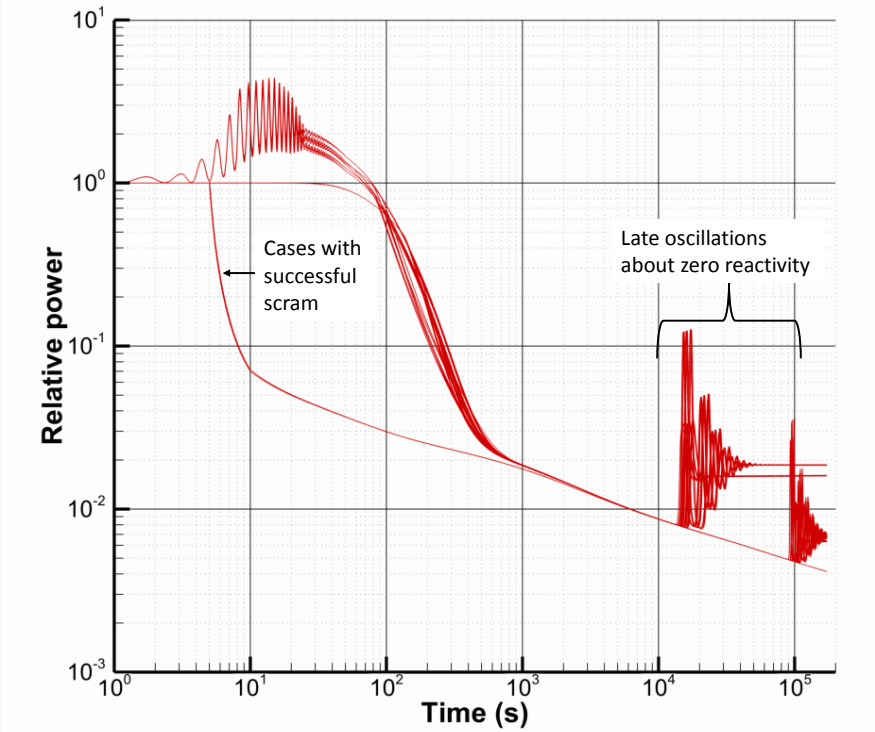

Figure 5.20. Relative power level for event tree simulation.

The peak temperatures due to the power excursion are not as severe as those from the sensitivity analysis in Section 5.1. The event tree has multipliers on the reactivity coefficients that are closer to 1.0, and the maximum multiplier on the positive sodium coefficient is only 1.34. Likewise, no branches encounter significant boiling and fuel damage during the reactivity excursion. Fuel failures in the event tree only occur after 10^4 s due to long-term deficiency in the decay heat removal by the DRACS in some scenarios; these failures are discussed more in the following paragraphs and sections.

The coolant temperature for some of the blue failure branches in Figure 5.22 do not quite reach the saturation temperature of the sodium coolant before the code is terminated, which is signified by the instantaneous drop to zero temperature. This is an artifact of the plotting frequency and the fact that SAS4A is predicting a very rapid temperature escalation just before coolant boiling and fuel relocation. The rapid temperature escalation can be seen in some of the blue branches in the upper-right corners of Figure 5.21 and Figure 5.22.

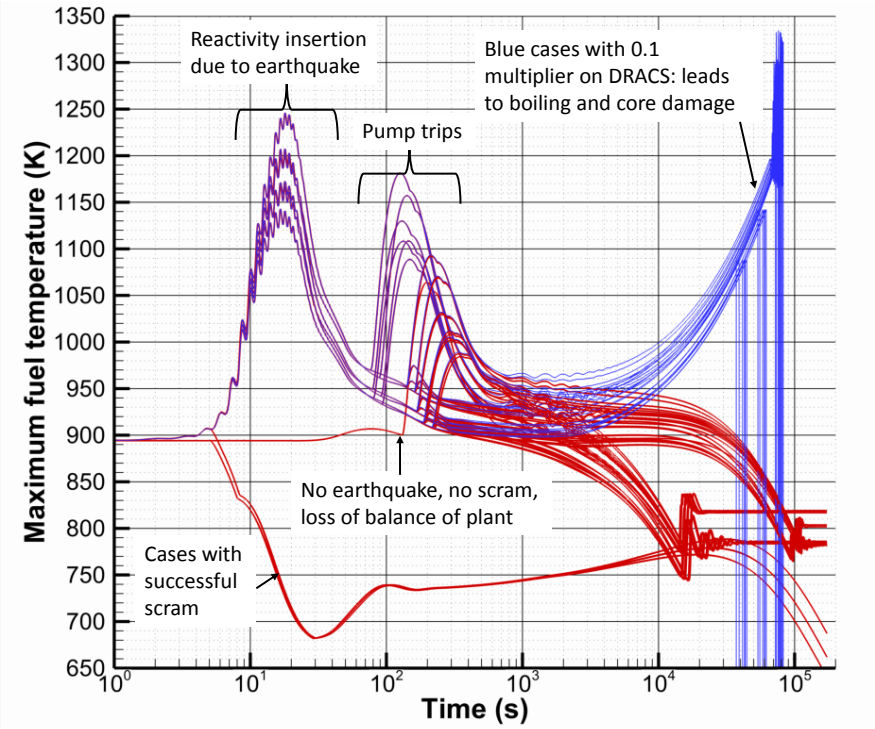

Figure 5.21. Maximum fuel temperature for event tree simulation.

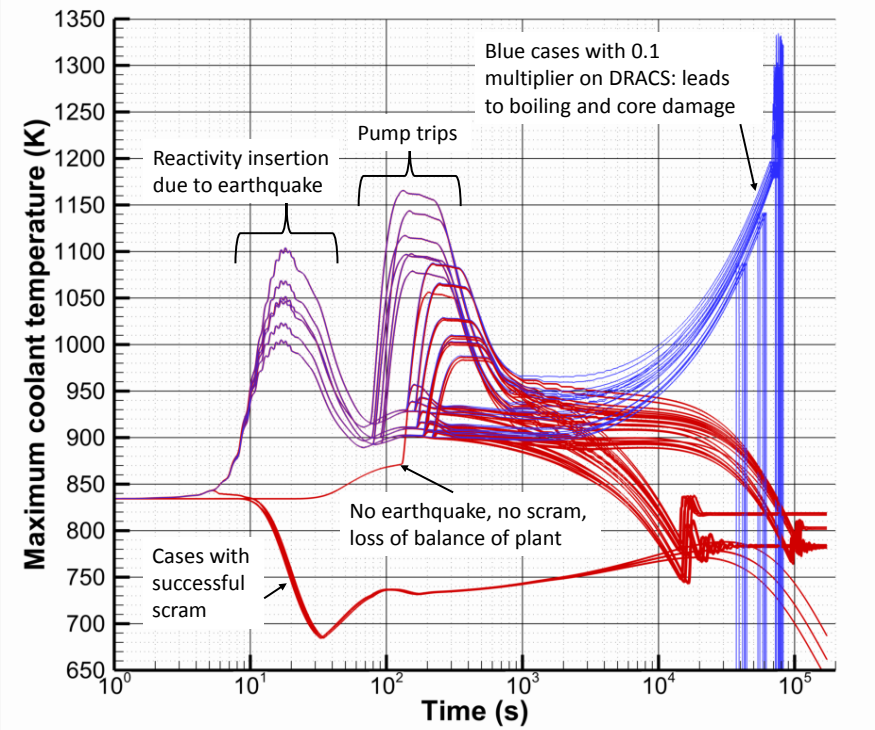

Figure 5.22. Maximum coolant temperature for event tree simulation.

The power to flow ratio, normalized to the steady-state value, for the event tree is depicted in Figure 5.23. Absolute flow rate in the inner core (channel 1) is a good indicator of the flow rate evolution for the core, as shown in Figure 5.24. The key features of the power to flow figure are quite intuitive and labeled on the plot. The late fluctuations in the red curves are mostly due to changes in power level caused by reactivities oscillating about zero. Most of the blue curves with fuel failures exhibit wild fluctuations in flow rate and power-to-flow ratio due to coolant boiling and flow reversals in the channels. Other failure branches do not show this trend due to early termination of the calculations, which is again an artifact of the plotting frequency and the rapid onset of severe channel disruption.

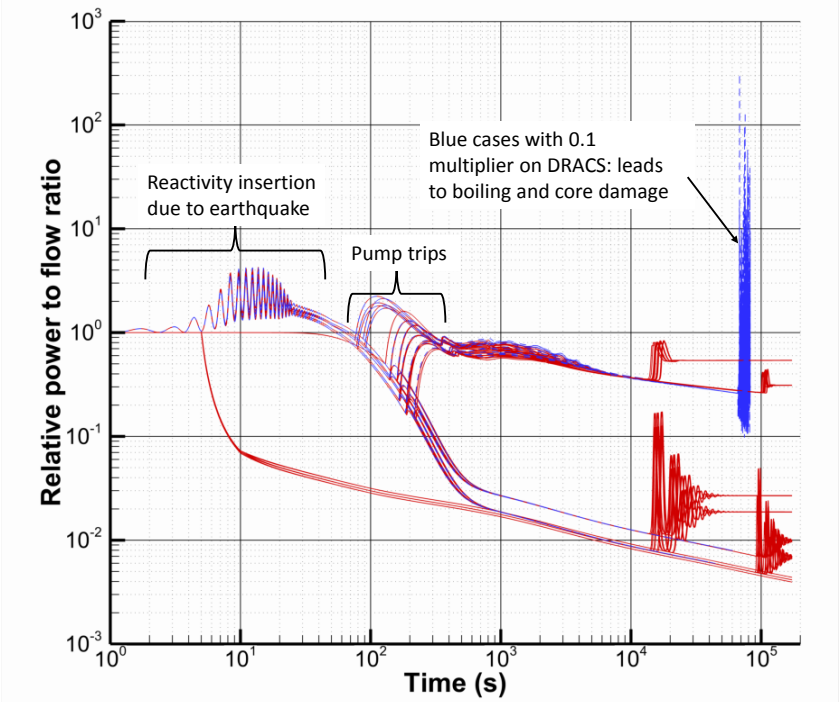

Figure 5.23. Relative power to flow ratio for event tree simulation.

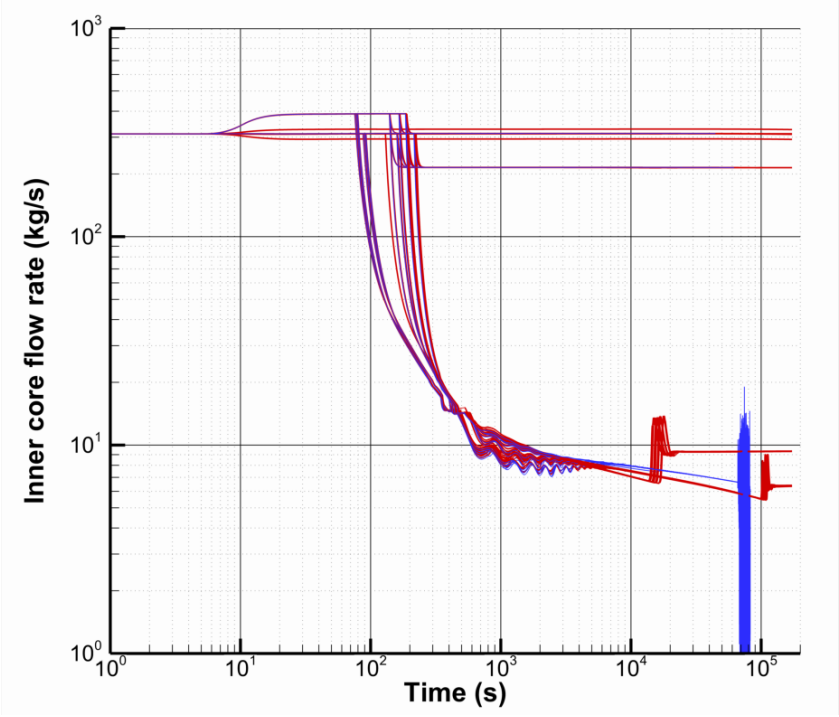

Figure 5.24. Inner core (channel 1) flow rate for event tree simulation.

5.2.2 Reactivity Feedback

The principal aspects of reactivity feedback during the power excursion were discussed in Section 5.1.2 for the sensitivity study. The initial stages (the power excursion) of the accident branches in the event tree are the same, and thus these features are not reviewed here. Instead, plots of reactivity feedback for the event tree are shown here to illustrate the reactivity and power trends associated with long-term cooling by DRACS and the reactivity signatures of the branches with successful scram.

Reactivity feedback is shown for the coolant, radial expansion, axial expansion, and Doppler feedback mechanisms by Figure 5.25, Figure 5.26, Figure 5.27, and Figure 5.28. Branches with scram show up with inverse feedback trends due to the immediate drop in core temperatures. The scram branches initially have negative sodium feedback and positive feedback for the other mechanisms, which is the reverse behavior of the accident branches. Each feedback component in the red accident branches is nearly zero by the end of the simulation; the small nonzero remainders of each feedback component sums to zero after 10^4 s in these cases, as shown in plot of total reactivity (Figure 5.19).

The branches with degraded DRACS and late-term fuel failures are again the blue curves in these figures. The gradual heatup of the plant after 1000 s results in considerable (> 0.2$) sodium feedback, but this positive feedback is easily countered by the negative axial/radial expansion and Doppler feedback due to increased core temperatures. Therefore, total reactivity in the fuel failure branches is much less than zero after 1000 s, and the onset of coolant boiling and channel distribution is the consequence of insufficient, long-term heat removal by DRACS and not because of a late reactivity/power excursion. The heat generation in the core at this time period is only due to decay heating by radionuclides. After the onset of sodium boiling, however, several branches predict very rapid insertions of positive reactivity (due to void feedback) just before the calculation terminates. Such signatures can be seen in the upper-right portion of Figure 5.25 for certain branches around $7x10^4$ s. Other branches with coolant boiling and fuel failure do not show this feature due to the plotting frequency of the data. Despite this rapid and positive void feedback, total reactivity appears to remain below zero for failure branches, as shown in Figure 5.19. Further, these branches do not exhibit late power fluctuations. (The late power oscillations in Figure 5.20 are the branches that do not have fuel failure, where total reactivity gradually returns to zero due to long-term cooling by DRACS.)

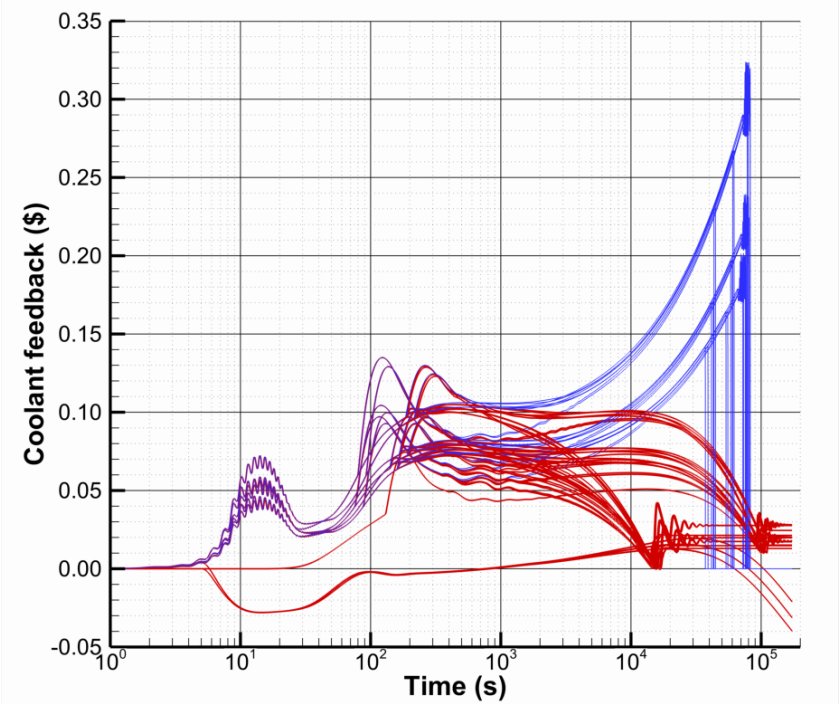

Figure 5.25. Coolant reactivity feedback for event tree simulation.

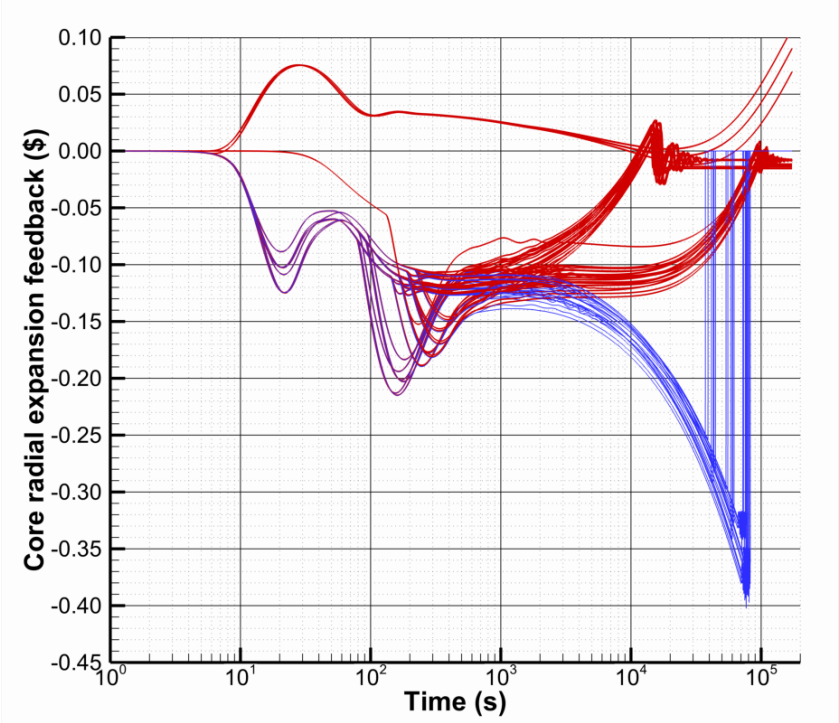

Figure 5.26. Radial expansion reactivity feedback for event tree simulation.

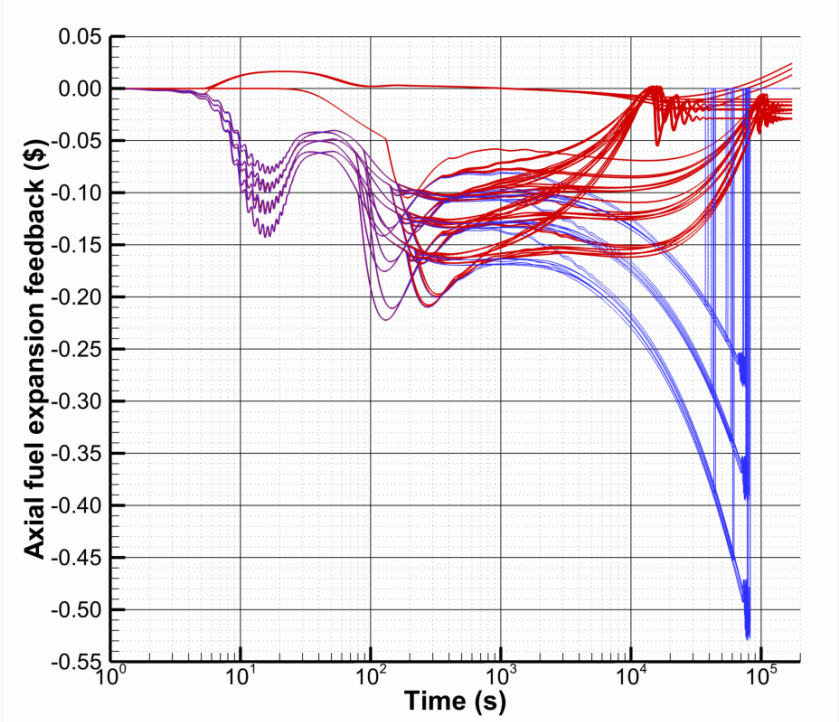

Figure 5.27. Axial expansion reactivity feedback for event tree simulation.

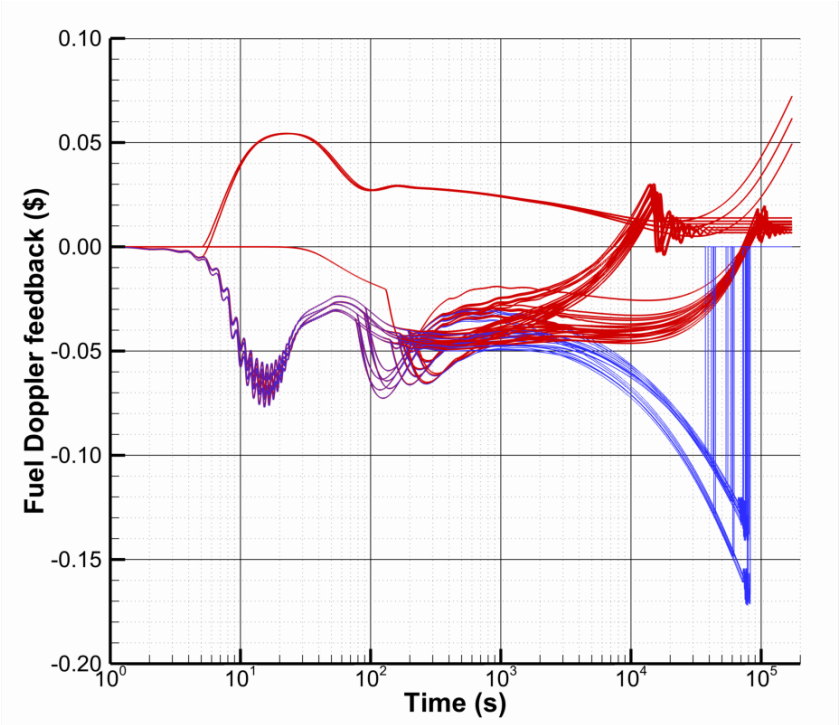

Figure 5.28. Doppler reactivity feedback for event tree simulation.

5.2.3 Eutectics and Cladding Thickness

The DEFORM5 models in SAS4A predict considerable thinning of the cladding due to fuel-cladding eutectics for the branches with the power excursion and subsequent pump trips. Minimum cladding thickness in the peak channel is depicted in Figure 5.29 for all branches in the event tree. The nominal branches (with scram), excluding the branch with no earthquake/scram, have essentially no reduction in cladding thickness over 48 hours. The blue curves in Figure 5.29 are now branches that predict cladding ruptures due to cladding wastage and increased internal pressure in the fuel elements. Four branches exhibit an early flat-line in cladding thickness (near 150 s) that signifies local cladding failure; additional cladding wastage and failures occur at lower axial levels in the peak channel and in the other channels, namely the inner core channel. Several other branches have local cladding failures followed by gross channel distribution, which is indicated by a sudden drop to zero cladding thickness. The 24 branches with degraded DRACS operation all lead to cladding failure, coolant boiling, and gross fuel failure.

Figure 5.29 demonstrates that several branches undergo cladding wastage over three distinct stages and over the course of many hours. Thus, cladding thickness is deemed to be a good integral measure of the severity of the accident. The periods of cladding wastage correspond to the three main stages of the accident progression: early reactivity excursion (1-50 s), pump trips (after 80 s), and gradual heat removal by the DRACS from 1000 s to 48 h. Many branches have extensive thinning of the cladding, with a few near 80% of the original thickness, after 48 h yet do not predict cladding rupture.

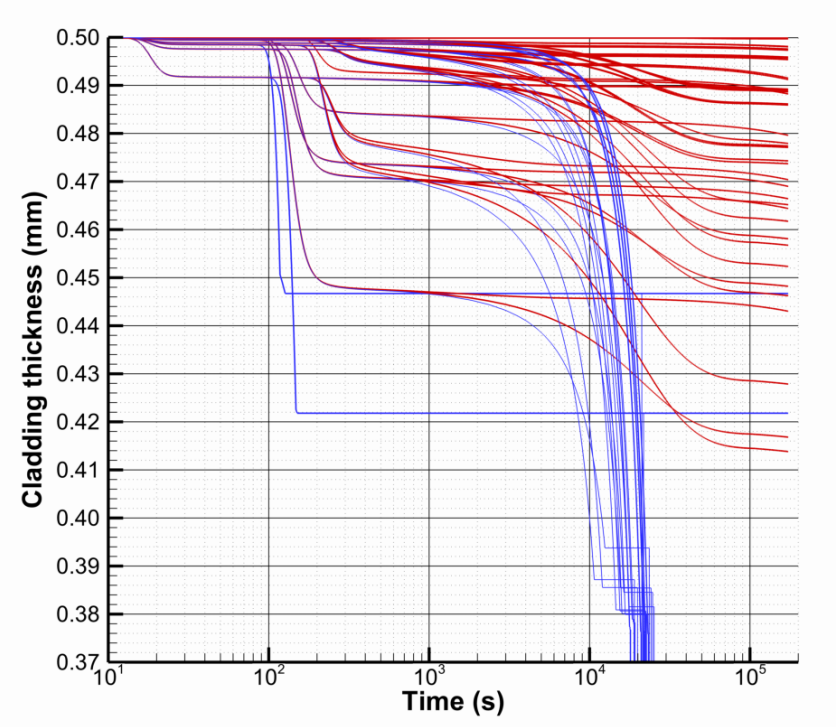

Figure 5.29. Cladding thickness for event tree simulation; top node of peak channel.

5.2.4 Accident Progression and Results Review

The essential features and outputs of each branch are amenable to summarization by a large table since the event tree only consists of 83 branches. Table 5.2 lists the branch indices, branch conditions, and some key results predicted by SAS4A. The abbreviations in Table 5.2 for the branch conditions are:

- **A**: Does the earthquake reactivity insertion occur or not;
- **B**: Does scram occur or not;
- **C**: Multiplier on primary pump torque that starts at 5 s into the accident;
- **D**: Multiplier on ADHX heat transfer coefficient (affects DRACS performance);
- **E**: Group number for reactivity coefficient multipliers (see Section 3.1.2);
- **F**: Do the operators manually trip the pumps once the cold pool reaches 798 K;
- **G**: Multiplier on primary pump torque if thermal pump failure occurs at 878.5 K.

Branch parameters C, D, and F reflect operator actions. For the SAS4A results in Table 5.2, pump trip entries may read 'no' or 'yes' followed by a letter that describes the trip mode of the pump. The letter 'O' denotes pump trip due to operator intervention, and the letter 'T' denotes thermal pump failure. The 'Cladding fail?' column indicates whether cladding rupture occurs or not, which is independent of the status of the fuel; i.e. four branches have cladding failure but not bulk coolant boiling and fuel failure. The 'Fuel fail?' column indicates whether boiling and fuel failure/relocation occurs, which terminates the simulation before 48 h. Only branches with the 0.1 multiplier on the ADHX heat transfer coefficient (column D in Table 5.2) reach such an end state. For these failure branches, the listed maximum coolant and fuel temperatures may not really be the true peak values due to the rapid temperature escalation that causes the channel disruption and the relatively coarse plotting frequency of the data. Furthermore, the cladding thickness column only reflects the minimum cladding thickness in the peak channel before rupture of the cladding. DEFORM5 stops printing data for a channel/node following local cladding failure, and the top node of the peak channel always undergoes cladding failure first.

Table 5.2. Event tree summary.

Branch conditions								SAS4A results						
#	A	B	C	D	E	F	G	Pump trip?	Pump trip time (s)	Max. Na Temp. (K)	Max Fuel Tem (K)	Cladding Th. (mm)	Cladding fail?	Fuel fail?
1	No	Yes	1	1	1	Yes	0	No	--	834.42	894.19	0.4998	no	no
2	No	Yes	1.1	1	1	Yes	0	No	--	834.42	894.19	0.4998	no	no
3	No	Yes	0.9	1	1	Yes	0	No	--	834.42	894.19	0.4998	no	no
4	No	Yes	1	1.1	1	Yes	0	No	--	834.42	894.19	0.4999	no	no
5	No	Yes	1	0.9	1	Yes	0	No	--	834.42	894.19	0.4997	no	no
6	No	No	1	1	1	Yes	0	yes, O	132.1	1056.30	1064.10	0.4779	no	no
7	Yes	Yes	1	1	1	Yes	0	No	--	843.21	907.31	0.4998	no	no
8	Yes	Yes	1.1	1	1	Yes	0	No	--	843.21	907.31	0.4998	no	no
9	Yes	Yes	0.9	1	1	Yes	0	No	--	843.21	907.31	0.4998	no	no
10	Yes	Yes	1	1.1	1	Yes	0	No	--	843.21	907.31	0.4999	no	no
11	Yes	Yes	1	0.9	1	Yes	0	No	--	843.21	907.31	0.4997	no	no
12	Yes	No	1	1	1	Yes	0	yes, O	89.9	1143.70	1246.20	0.4218	yes	no
13	Yes	No	1.5	1	1	Yes	0	yes, O	79.7	1165.50	1207.60	0.4467	yes	no
14	Yes	No	1	10	1	Yes	0	yes, O	89.9	1143.70	1246.20	0.4218	yes	no

Table 5.2. Event tree summary. (Continued)

#	A	B	C	D	E	F	G	Pump trip?	Pump trip time (s)	Max. Na Temp. (K)	Max Fuel Tem (K)	Cladding Th. (mm)	Cladding fail?	Fuel fail?
15	Yes	No	1.5	10	1	Yes	0	yes, O	79.7	1165.50	1207.60	0.4467	yes	no
16	Yes	No	1	0.1	1	Yes	0	yes, O	89.9	1334.60	1334.60	0.4218	yes	yes
17	Yes	No	1.5	0.1	1	Yes	0	yes, O	79.7	1299.50	1299.70	0.4467	yes	yes
18	Yes	No	1	1	2	Yes	0	yes, O	92.5	1097.50	1201.30	0.4482	no	no
19	Yes	No	1.5	1	2	Yes	0	yes, O	81.9	1117.10	1168.80	0.4168	no	no
20	Yes	No	1	10	2	Yes	0	yes, O	92.5	1097.50	1201.30	0.4664	no	no
21	Yes	No	1.5	10	2	Yes	0	yes, O	81.9	1117.10	1168.80	0.4430	no	no
22	Yes	No	1	0.1	2	Yes	0	yes, O	92.5	1327.50	1327.40	0.3854	yes	yes
23	Yes	No	1.5	0.1	2	Yes	0	yes, O	81.9	1331.10	1331.10	0.3938	yes	yes
24	Yes	No	1	1	3	Yes	0	yes, O	94.2	1078.80	1172.80	0.4581	no	no
25	Yes	No	1.5	1	3	Yes	0	yes, O	83.4	1096.70	1143.00	0.4463	no	no
26	Yes	No	1	10	3	Yes	0	yes, O	94.2	1078.80	1172.80	0.4796	no	no
27	Yes	No	1.5	10	3	Yes	0	yes, O	83.4	1096.70	1143.00	0.4690	no	no
28	Yes	No	1	0.1	3	Yes	0	yes, O	94.2	1299.20	1299.70	0.3815	yes	yes
29	Yes	No	1.5	0.1	3	Yes	0	yes, O	83.4	1323.70	1323.70	0.3845	yes	yes
30	Yes	No	1	1	1	No	0	yes, T	161.7	1104.20	1246.20	0.4279	no	no
31	Yes	No	1	1	1	No	0.5	yes, T	165.3	1104.20	1246.20	0.4737	no	no
32	Yes	No	1	1	1	No	1	No	--	1104.20	1246.20	0.4743	no	no
33	Yes	No	1.5	1	1	No	0	yes, T	143.8	1087.30	1207.60	0.4138	no	no
34	Yes	No	1.5	1	1	No	0.5	yes, T	148.5	1051.90	1207.60	0.4771	no	no
35	Yes	No	1.5	1	1	No	1	No	--	1051.90	1207.60	0.4774	no	no
36	Yes	No	1	10	1	No	0	yes, T	162.9	1104.20	1246.20	0.4704	no	no
37	Yes	No	1	10	1	No	0.5	yes, T	166.5	1104.20	1246.20	0.4891	no	no
38	Yes	No	1	10	1	No	1	No	--	1104.20	1246.20	0.4892	no	no
39	Yes	No	1.5	10	1	No	0	yes, T	144.3	1086.40	1207.60	0.4644	no	no
40	Yes	No	1.5	10	1	No	0.5	yes, T	149.1	1051.90	1207.60	0.4954	no	no
41	Yes	No	1.5	10	1	No	1	No	--	1051.90	1207.60	0.4955	no	no
42	Yes	No	1	0.1	1	No	0	yes, T	161.2	1332.80	1332.70	0.3855	yes	yes
43	Yes	No	1	0.1	1	No	0.5	yes, T	164.8	1142.00	1246.20	0.3789	yes	yes
44	Yes	No	1	0.1	1	No	1	yes, T	39100.0	1104.20	1246.20	0.3783	yes	yes
45	Yes	No	1.5	0.1	1	No	0	yes, T	143.4	1300.70	1301.10	0.3872	yes	yes
46	Yes	No	1.5	0.1	1	No	0.5	yes, T	148.2	1142.00	1207.60	0.3774	yes	yes
47	Yes	No	1.5	0.1	1	No	1	yes, T	37300.0	1087.90	1207.60	0.3768	yes	yes
48	Yes	No	1	1	2	No	0	yes, T	194.3	1069.00	1201.30	0.4568	no	no
49	Yes	No	1	1	2	No	0.5	yes, T	197.9	1069.00	1201.30	0.4859	no	no
50	Yes	No	1	1	2	No	1	No	--	1069.00	1201.30	0.4861	no	no
51	Yes	No	1.5	1	2	No	0	yes, T	169.7	1028.20	1168.80	0.4523	no	no
52	Yes	No	1.5	1	2	No	0.5	yes, T	174.4	1023.50	1168.80	0.4859	no	no
53	Yes	No	1.5	1	2	No	1	No	--	1023.50	1168.80	0.4861	no	no
54	Yes	No	1	10	2	No	0	yes, T	197.6	1069.00	1201.30	0.4887	no	no
55	Yes	No	1	10	2	No	0.5	yes, T	201.2	1069.00	1201.30	0.4958	no	no
56	Yes	No	1	10	2	No	1	No	--	1069.00	1201.30	0.4959	no	no
57	Yes	No	1.5	10	2	No	0	yes, T	171.5	1026.50	1168.80	0.4882	no	no
58	Yes	No	1.5	10	2	No	0.5	yes, T	176.3	1023.50	1168.80	0.4975	no	no
59	Yes	No	1.5	10	2	No	1	No	--	1023.50	1168.80	0.4976	no	no
60	Yes	No	1	0.1	2	No	0	yes, T	192.8	1299.10	1299.10	0.3807	yes	yes

Table 5.2. Event tree summary. (Continued)

#	A	B	C	D	E	F	G	Pump trip?	Pump trip time (s)	Max. Na Temp. (K)	Max Fuel Tem (K)	Cladding Th. (mm)	Cladding fail?	Fuel fail?
61	Yes	No	1	0.1	2	No	0.5	yes, T	196.4	1142.10	1201.30	0.3765	yes	yes
62	Yes	No	1	0.1	2	No	1	yes, T	42900.0	1088.00	1201.30	0.3758	yes	yes
63	Yes	No	1.5	0.1	2	No	0	yes, T	168.9	1330.50	1330.60	0.3809	yes	yes
64	Yes	No	1.5	0.1	2	No	0.5	yes, T	173.7	1142.00	1168.80	0.3763	yes	yes
65	Yes	No	1.5	0.1	2	No	1	yes, T	41500.0	1088.00	1168.80	0.3757	yes	yes
66	Yes	No	1	1	3	No	0	yes, T	219.7	1047.20	1172.80	0.4652	no	no
67	Yes	No	1	1	3	No	0.5	yes, T	223.3	1047.20	1172.80	0.4891	no	no
68	Yes	No	1	1	3	No	1	No	--	1047.20	1172.80	0.4892	no	no
69	Yes	No	1.5	1	3	No	0	yes, T	190.4	1005.20	1143.00	0.4617	no	no
70	Yes	No	1.5	1	3	No	0.5	yes, T	195.1	1005.20	1143.00	0.4887	no	no
71	Yes	No	1.5	1	3	No	1	No	--	1005.20	1143.00	0.4889	no	no
72	Yes	No	1	10	3	No	0	yes, T	225.5	1047.20	1172.80	0.4915	no	no
73	Yes	No	1	10	3	No	0.5	yes, T	229.0	1047.20	1172.80	0.4973	no	no
74	Yes	No	1	10	3	No	1	No	--	1047.20	1172.80	0.4974	no	no
75	Yes	No	1.5	10	3	No	0	yes, T	193.4	1005.20	1143.00	0.4912	no	no
76	Yes	No	1.5	10	3	No	0.5	yes, T	198.2	1005.20	1143.00	0.4980	no	no
77	Yes	No	1.5	10	3	No	1	No	--	1005.20	1143.00	0.4981	no	no
78	Yes	No	1	0.1	3	No	0	yes, T	217.0	1332.10	1332.10	0.3799	yes	yes
79	Yes	No	1	0.1	3	No	0.5	yes, T	220.6	1142.10	1172.80	0.3759	yes	yes
80	Yes	No	1	0.1	3	No	1	yes, T	44600.0	1088.00	1172.80	0.3752	yes	yes
81	Yes	No	1.5	0.1	3	No	0	yes, T	188.9	1331.30	1332.80	0.3801	yes	yes
82	Yes	No	1.5	0.1	3	No	0.5	yes, T	193.7	1142.00	1143.00	0.3759	yes	yes
83	Yes	No	1.5	0.1	3	No	1	yes, T	43400.0	1088.00	1143.00	0.3753	yes	yes

5.3 References

[5.1] Argonne National Laboratory, Nuclear Engineering Division "The SAS4A/SASSYS-1 Safety Analysis Code System," ANL/NE-12/4, Argonne National Laboratory, Argonne, IL, 2011.

[5.2] K. A. El-Sheikh, "Probabilistic Risk Assessment of the Advanced Liquid Metal Reactor," GE Nuclear Energy. GEFR-00873, 1994.

[5.3] A. M. Tentner et al., "Severe Accident Approach – Final Report Evaluation of Design Measures for Severe Accident Prevention and Consequence Mitigation," ANL-GENIV-128, Argonne National Laboratory, Argonne, IL, 2010.

6 SUMMARY

This report describes a severe accident management study for a small sodium reactor subjected to a 0.5g seismic event. A primary goal of this study was to analyze a beyond design basis accident in a dynamic event tree framework, exploring both the impact of uncertainties and human intervention, in order to provide operational insights to reduce potential for reactor damage. These objectives were accomplished. Another goal of this study was to use the insights from the accident analysis to create a BN which can learn from the instrumented variables with the objective of inferring key states of the reactor. This objective was also accomplished. A third goal of this study was to use the BN to provide example inferences throughout the progression tree. This objective will be accomplished in follow-on research in FY15 under the DOE Advanced Reactor Concepts Work Package AT-15SN200304.

6.1 Key results

The overarching result from this report is that the small sodium fast reactor analyzed here-in is extremely robust to beyond design basis accidents. With the DRACS system working as designed, fuel melting is avoided in every accident progression tree branch. However, high sustained cladding temperatures can occur after a subsequent loss of flow due to excessive cold pool temperature rising above the primary pump trip set point (i.e., 525^{o}C). Two operator actions were considered to reduce the potential of cladding damage for this sequence: (1) modifying the DRACS system by inserting water to the air inlet and (2) overriding the primary pump trip set point.

The first accident management option is to increase the DRACS heat transfer rate by inserting water into the air inlet. This was modeled by increasing the DRACS heat transfer coefficient by an order of magnitude, an approximation which could obviously be improved by supplemental external calculations. This action staved off cladding failure for all accident progression branches except those involving the most unfavorable reactivity coefficients. From a correlated uncertainty study conducted separately from the accident progression tree analysis, this set of reactivity coefficients has an 8% chance of occurring.

Inserting water into the DRACS also introduces a potential failure mode for the DRACS because the operation of the system would exceed the design envelope of the DRACS. Failure of the DRACS was modeled by reducing the heat transfer coefficient by an order of magnitude, an approximation which again could be improved by supplemental external calculations. If the DRACS were to fail, fuel melting and cladding failure would be expected for every accident branch. The accident progression trees and the BN are not sufficiently developed to determine the optimal conditions for supplementing DRACS. Analyses of additional earthquake induced transients will be needed to assess the overall viability of this accident management method.

The second accident management option is to override the primary pump trip set point and allow the EM pumps to run until they overheat, in which case they would fail at the overheat temperature. It should be noted that a significant number of accident branches extended beyond the trip set point, but the inherent feedbacks in the reactor prevented subsequent pump failures. Endangering the pumps prevented the cladding failure end state while not opening the door to fuel failure, except for the branches where failed DRACS resulted in fuel failure.

In summary, enhancing DRACS has both greater upside and downside than overriding the EM pump set point when it comes to preservation of the core, but both can reduce core damage. The optimal strategy will depend on what state the operators infer (via the BN) the reactor to be in before they respond.

6.2 Future work

6.2.1 Bayesian Network Inferencing

The initial Bayesian Network structure shows significant potential to support diagnosis and provide evidence-based insights into the value of different monitored parameters. Additional work is required before the BN model can be used to conduct activities related to inference on the variables in the model, including real-time decision support and further examination of SFR accident characteristics. Near-term BN development activities are focused on integrating the results from Section 5 into the model and subsequently performing inference on monitored parameters.

Additional efforts will also explore options for automating the quantification of the BN model using SAS4a results; this is a critical step in expanding the prototype model to include the extensive range of accident situations that must be represented in a SAMG.

6.2.2 Expansion of the accident progression trees

Additional accident sequence scope will be added in future work, which will also lead to additional expansion of the BN model to demonstrate the ability for the BN model to reason across a larger accident suite. Multi-site risk issues researched conducted at ORNL can be used to help inform prior uncertainties in the BN so that the impact of those uncertainties upon multi-site risk can be studies and those uncertainties and be prioritized for scrutiny in severe accident management strategies.

Decay heat removal experiments at ANL in both normal and degraded configurations will provide insights for developing branch point uncertainties in the DDET accident analyses. The DDET/BN decision support structure will be exercised to identify how these uncertainties could influence accident management. These results will help prioritize future experiments and tests. Future DDET/BN analyses will examine the impact of water ingress into air heat removal, which could inform the need for high fidelity models being developed at INL. In the event that ANL test schedules slip past the point for incorporation into SNL DDET analyses, parametric sensitivity analyses will be performed to simulate the potential impact of phenomenological uncertainties related to the heat removal experiments, and experimental results would then be incorporated into future work.

6.3 Impact on Regulatory Acceptability of SFRs

As advanced reactors, for which there exists less operational experience than for LWRs, move toward risk-informed licensing, regulatory attention could be focused upon the formulation of annual probability of occurrence uncertainties. As was seen in Figure 1.1, radiological risk

profiles for SFRs can exhibit cliff-edges in occurrence probability-consequence space. The relatively flat “risk plateau” to the left of theses cliff edges may be problematic for risk-informed design certification or licensing because annual occurrence probabilities for rare external events, events which can cause cliff-edges, are often characterized with large uncertainties. These uncertainties can potentially span regions of regulatory interest.

Accident management can be utilized to increase the slope of these “risk plateaus” and soften the cliff-edge effect of SFR risk profiles. By planning for accident management of rare events before licensing, reactor licensees can make the case to the regulatory that one event does not mean the difference between no public consequences and large public consequences.

BIBLIOGRAPHY

- D. Helton (2009). "Scoping Study on Advancing Modeling Techniques for Level 2/3 PRA," U.S. Nuclear Regulatory Commission, May 2009. Available via the US NRC's ADAMS at accession no. ML091320454.
- Argonne National Laboratory, Nuclear Engineering Division (2011) "The SAS4A/SASSYS-1 Safety Analysis Code System," ANL/NE-12/4, Argonne National Laboratory, Argonne, IL.
- M. Denman et al. (2013). "Discrete Dynamic Event Tree Capability Study for Advanced Small Modular Reactors," SAND2013-2514, Sandia National Laboratories: Albuquerque, NM.
- Y. H. J. Chang & A. Mosleh (2007). "Cognitive modeling and dynamic probabilistic simulation of operating crew response to complex system accidents: Part 5: Dynamic probabilistic simulation of the IDAC model." *Reliability Engineering and System Safety*, **92**, 1076-1101.
- D. Kunsman, et al. (2008). "Development and Application of the Dynamic System Doctor to Nuclear Reactor Probabilistic Risk Assessments," SAND2008-4746, Sandia National Laboratories, Albuquerque, NM.
- J. Persensky et al., "Guidance for Assessing Exemption Requests from the Nuclear Power Plant Licensed Operator Staffing Requirements Specified in 10 CFR 50.54(m)," NUREG-1791, U.S. Nuclear Regulatory Commission, Washington, DC, July 2005.
- "Operator Staffing for Small or Multi-Module Nuclear Power Plant Facilities," SECY-11-0098, U.S. Nuclear Regulatory Commission, Washington, DC, July 2011.
- J. LaChance, et al. (2013). "Evaluation of the Applicability of Existing Nuclear Power Plant Regulatory Requirements in the U.S. to Advanced Small Modular Reactors," SAND2013-3683, Sandia National Laboratories, Albuquerque, NM.
- H. Liao et al. (2013). "Leveraging Existing Tools for Simulating Operator Performance In discrete Dynamic Event Trees." SAND2013-3818C, Sandia National Laboratories, Albuquerque, NM.
- C. Miller, et al. (2011). "Recommendations for Enhancing Reactor Safety in the 21st Century: The Near-Term Task Force Review of Insights from the Fukushima Dai-Ichi Accident." U.S. Nuclear Regulatory Commission, July 2011. Available via the US NRC's ADAMS at accession no. ML111861807.
- J. Pearl (2000). *Causality: models, reasoning, and inference.* Cambridge University Press.
- M. Druzdzel and F. Díez (2003). "Combining knowledge from different sources in causal probabilistic models." *Journal of Machine Learning Research*, 4, 295-316.
- U.S. NRC, "State-of-the-Art Reactor Consequence Analyses Project, Uncertainty Analysis of the Unmitigated Long-Term Station Blackout of the Peach Bottom Atomic Power Station," NUREG/CR-7155, DRAFT REPORT (SAND2012-10702P), 2012.

- GeNIe software (2003). University of Pittsburgh Decision Systems Laboratory. http://genie.sis.pitt.edu
- R. M. Jagt (2002). *Support for Multiple Cause Diagnosis with Bayesian Networks.* Master's Thesis. Delft University of Technology, Delft, Netherlands.

SAND2015-2484

DISTRIBUTION

Internal Distribution (electronic copy)

1	MS0748	Jeff Cardoni	6232
1	MS0748	Matthew R. Denman	6231
1	MS0748	Katrina M. Groth	6231
1	MS0748	Tim Wheeler	6231
1	MS0899	Technical Library	9536


Sandia National Laboratories